

Numerical Simulations of Island Effects on Airflow and Weather during the Summer over the Island of Oahu

HIEP VAN NGUYEN AND YI-LENG CHEN

Department of Meteorology, University of Hawaii at Manoa, Honolulu, Hawaii

FRANCIS FUJIOKA

Pacific Southwest Research Station, USDA Forest Service, Riverside, California

(Manuscript received 25 August 2009, in final form 22 December 2009)

ABSTRACT

The high-resolution (1.5 km) nonhydrostatic fifth-generation Pennsylvania State University–National Center for Atmospheric Research (PSU–NCAR) Mesoscale Model (MM5) and an advanced land surface model (LSM) are used to study the island-induced airflow and weather for the island of Oahu, Hawaii, under summer trade wind conditions.

Despite Oahu's relatively small area (1536 km²), there are considerable spatial variations in horizontal distribution of thermodynamic fields related to terrain, airflow, rain, cloud, and ground cover. The largest diurnal variations in temperature and moisture occur in the lee sides of mountains, especially along the western leeside coast. The island-scale surface airflow is also significantly affected by terrain and land surface forcing. The downslope winds above the leeside slopes of both the Ko'olau and Waianae Mountains are simulated with significant diurnal variations with the strongest downslope winds just before sunrise.

The timing of diurnal rainfall maxima over the Ko'olau Mountains is closely related to vertical motions. The early morning rainfall maximum on the windward side is caused by anomalous rising motion due to significant flow deceleration when the land surface is the coolest. The evening rainfall maximum after sunset is related to anomalous orographic lifting due to stronger winds aloft. In the early afternoon, winds aloft are relatively weak with a relatively high level of free convection (LFC) because of vertical mixing. As a result, the rainfall over the Ko'olau Mountains exhibits an afternoon minimum. The westerly reversed flow off the western leeside coast in the afternoon is mainly thermally driven and related to land surface heating superimposed by latent heat release of persistent orographic precipitation over the Ko'olau Mountains. Rainfall along the western leeside slopes has a late afternoon maximum due to the development of the onshore/upslope flow.

1. Introduction

On a global scale, rainfall in the trade wind belt is minimal. However, rainfall over the Hawaiian Islands is frequent and abundant (Schroeder et al. 1977) because of terrain and local trade wind interactions. Hawaii's array of microclimates, ranging from its humid and tropical windward flanks to dry and sometimes desertlike leeward areas (Giambelluca et al. 1986), make it an ideal laboratory for the study of the atmospheric response of airflow to island size, shape, mountain height, and surface properties.

The relatively uniform trade wind flow from the open ocean is distorted and disrupted by the mountains, hills, and valleys of the islands. In the past, most high-resolution datasets for mountainous islands were collected during field experiments. For the Hawaiian Islands, special field studies have been conducted mainly over the island of Hawaii. Besides lifting and orographic blocking (Smolarkiewicz et al. 1988), mountains also act as a heat source (sink) during the day (night; Leopold 1948, 1949). In regions with weak winds, surface heating induces upslope/onshore flow during the day and surface cooling yields downslope/offshore flow at night (Chen and Nash 1994; Feng and Chen 1998). On the windward side of the island of Hawaii, the early morning convergence of the orographically blocked trade winds (Smolarkiewicz et al. 1988) and the opposing katabatic flow significantly

Corresponding author address: Yi-Leng Chen, University of Hawaii at Manoa, 2525 Correa Rd., Honolulu, HI 96822.
E-mail: yileng@hawaii.edu

contribute to the nocturnal rainfall over the area (Chen and Nash 1994). Yang and Chen (2008) simulated low-level nocturnal convergence on the windward side of an island with the same horizontal area as the island of Hawaii, but with flat terrain. They found convergence on the windward side at night as a result of reduced wind speed over land caused by a combination of nocturnal cooling and surface friction.

Most of the previous theoretical studies on airflow past 3D mountains are based on theoretical studies (e.g., Smolarkiewicz et al. 1988; Smolarkiewicz and Rotunno 1989; Schär and Smith 1993; Rotunno et al. 1999; Schär and Durran 1997; Epifanio and Rotunno 2005). For $U/N > h$ (where N is the Brunt–Väisälä frequency, U is the upstream cross-mountain wind speed, and h is the mountain height), the surface air parcels flow almost directly over the mountain with a large-amplitude gravity wave over the peak (Smolarkiewicz et al. 1988; Smolarkiewicz and Rotunno 1989). For U/N much smaller than h , the low-level flow is diverted around the flanks of the mountain. These studies have shown that the Froude number ($Fr = U/Nh$) is the control parameter for the transition from the “flow over” to the “flow around” regime. These studies also show the clear link between the upstream blocking and the leeside wakes and vortices. Epifanio and Rotunno (2005) showed that blocking of the flow leads to the formation of a warm air anomaly over the leeside slope as potentially warmer air descends from aloft to replace the colder air deflected laterally around the barrier. The resulting negative temperature gradient between the warm leeslope air and the colder air downstream then leads to the flow reversal in the lee. Leopold (1949) showed that for mountains with tops well above the trade wind inversion (~ 2 km in Hawaii), the inversion serves as a lid forcing the low-level flow to be deflected by the terrain (Schär and Smith 1993). Chen and Feng (2001) showed that for the island of Hawaii with peaks well above the trade wind inversion, in addition to Fr , the island-scale airflow and weather are affected by the trade wind inversion height and net diabatic heating associated with clouds and precipitation. Yang et al. (2005) used the fifth-generation Pennsylvania State University–National Center for Atmospheric Research (PSU–NCAR) Mesoscale Model (MM5) coupled with an advanced land surface model (Chen and Dudhia 2001) with proper treatment of lower boundary conditions over land (Zhang et al. 2005a) to simulate the full diurnal cycles of island-induced airflow and weather over the island of Hawaii. They successfully simulated the thermally induced diurnal circulation cells and their interactions with the counter-rotating lee vortices off the coast. Carlis et al. (2010) successfully simulated the Maui Vortex over the Maui Central Valley in the lee of

Haleakala (height ~ 3055 m) as well as the impacts of land surface forcing over the island and orographic blocking of the West Maui Mountains on the size, location, horizontal extent, and diurnal evolution of the Maui vortex.

Although there are many studies of island effects on rainfall over the Hawaiian Islands, only a few focus on the island of Oahu (e.g., Loveridge 1924; Leopold 1948), where more than 80% of the state’s population resides. Oahu has two mountain ranges, the Ko’olau Mountains and the Waianae Mountains, with peaks of 960 and 1200 m, respectively. Both mountain ranges are below the normal trade wind inversion (TWI) height (~ 2 km) and are oriented nearly perpendicular to the mean easterly trade wind flow. Leopold (1949) suggested that the frequently observed nocturnal rainfall maximum over the windward side is possibly related to cloud-top radiative cooling and stronger winds aloft at night. In addition to the nocturnal rainfall on the windward side, there is a small afternoon maximum on the leeside coast (Leopold 1948). The recent deployment of weather stations and rain gauges around the state by the National Weather Service (NWS) and other agencies has resulted in 69 hourly rain gauge stations and 13 weather stations over Oahu. These stations allow the improved study of the effects of terrain and the diurnal heating cycle on Oahu’s weather. The data collected from these stations also enable the evaluation of high-resolution weather models, one of the main subjects of this study. Hartley and Chen (2010, hereafter HC) found that, in the early morning, flow deceleration on the windward coastal area is significant when the island land surface is at its coolest. Winds are calm over central Oahu before sunrise, with weak westerly katabatic winds on the windward side of the Waianae Mountains. Most stations over the Ko’olau Mountains have an early morning rainfall maximum and a secondary evening rainfall maximum. A small afternoon hourly rainfall frequency maximum is observed along the western lee side because of the development of the on-shore flow there.

Lavoie (1974) used a simple mesoscale model to study trade wind weather over Oahu. His model simulated hydraulic jumplike behavior over the lee of both mountains, but not the thermally driven land/sea-breeze circulations. Recently, Zhang et al. (2005a) used a nonhydrostatic mesoscale spectral model (MSM; Juang 2000) to simulate weather conditions at three major airport stations on Oahu, and found that an advanced land surface model (LSM) with adequate descriptions of vegetation and ground cover over Oahu was required to better simulate the diurnal variations of the island’s surface airflow and weather. They compared results of the regional spectral model (RSM) at a horizontal resolution of 10 km (Wang et al. 1998) with that of the high-resolution (1.5 km)

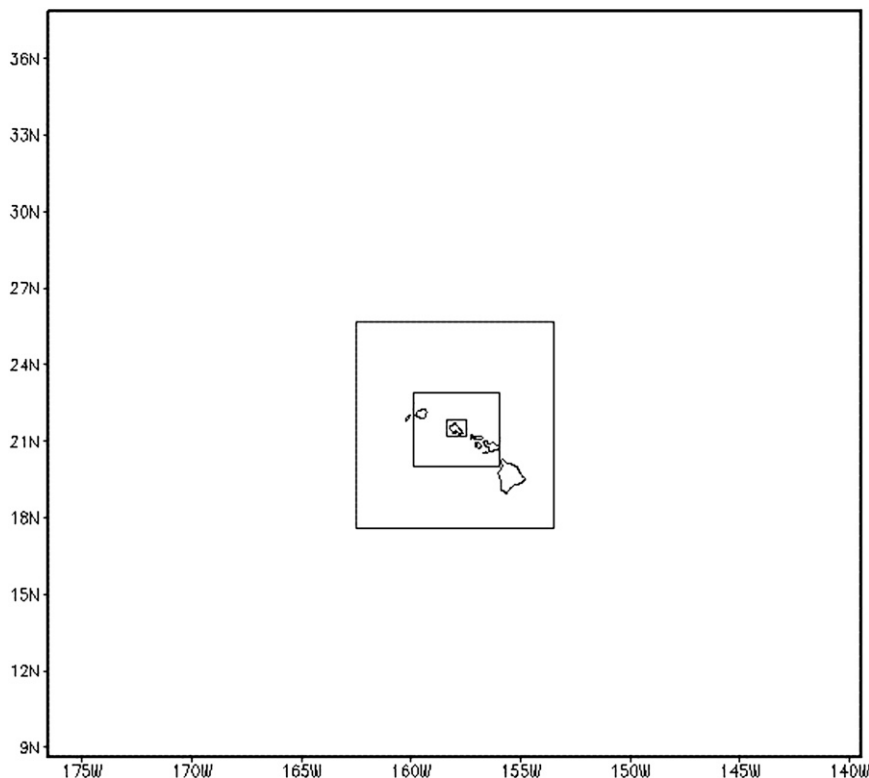


FIG. 1. The four domains employed in this study, with resolutions of 40.5, 13.5, 4.5, and 1.5 km, respectively.

MSM coupled with the Noah LSM, and determined that the MSM/LSM produced much better simulations than the RSM alone.

In this study, the high-resolution nonhydrostatic MM5 and the Noah LSM (Chen and Dudhia 2001) together with the vegetation cover and soil data compiled by Zhang et al. (2005a) are used to study the island-induced airflow and weather for the island of Oahu under summer trade wind conditions. The goals for this research are as follows: 1) to validate the MM5/LSM in simulating island-induced weather over Oahu; 2) to use the model as a tool to simulate island effects on surface airflow and rainfall over the island; and 3) to study the impact of terrain and daytime heating/nighttime cooling on airflow along the windward and leeside coasts, as well as the downslope winds aloft. The model results will be used to diagnose the physical processes responsible for the observed diurnal variations in rainfall. In addition, with mountain heights well below the trade wind inversion (~ 2 km), the observed westerly reversed flow in the leeside wake off the western Oahu coast during the day is apparently not in the same flow regime as wakes in the lee of high mountains (e.g., Yang et al. 2005; Carlis et al. 2010). In this study, model sensitivity tests will be performed to study the relative role of thermal forcing

versus orographic blocking on the development of westerly reversed flow in the leeside wake zone during the daytime.

2. Model descriptions

The MM5, a limited-area, nonhydrostatic, terrain-following sigma-coordinate model (Dudhia 1993), is used. Four nested domains are employed in the model with a two-way nesting, with horizontal resolutions of 40.5, 13.5, 4.5, and 1.5 km, and horizontal dimensions of 82×82 , 70×70 , 79×88 , and 52×64 , respectively (Fig. 1). The 1.5-km domain covers the entire island of Oahu. There are 28 vertical levels¹ from the surface to the 100-hPa level.

The physics options for the simulations are the same as those used in Yang et al. (2005) for the island of Hawaii, and include the Grell cumulus parameterization scheme (Grell, 1993), the medium-range forecast (MRF) planetary boundary layer scheme (Hong and Pan 1996), explicit warm rain microphysics (Hsie et al. 1984), and the

¹ The full sigma levels are 1.0, 0.998, 0.994, 0.990, 0.985, 0.980, 0.097, 0.945, 0.91, 0.865, 0.82, 0.79, 0.76, 0.72, 0.68, 0.63, 0.58, 0.52, 0.475, 0.425, 0.375, 0.325, 0.275, 0.225, 0.175, 0.125, 0.075, 0.025, and 0.0.

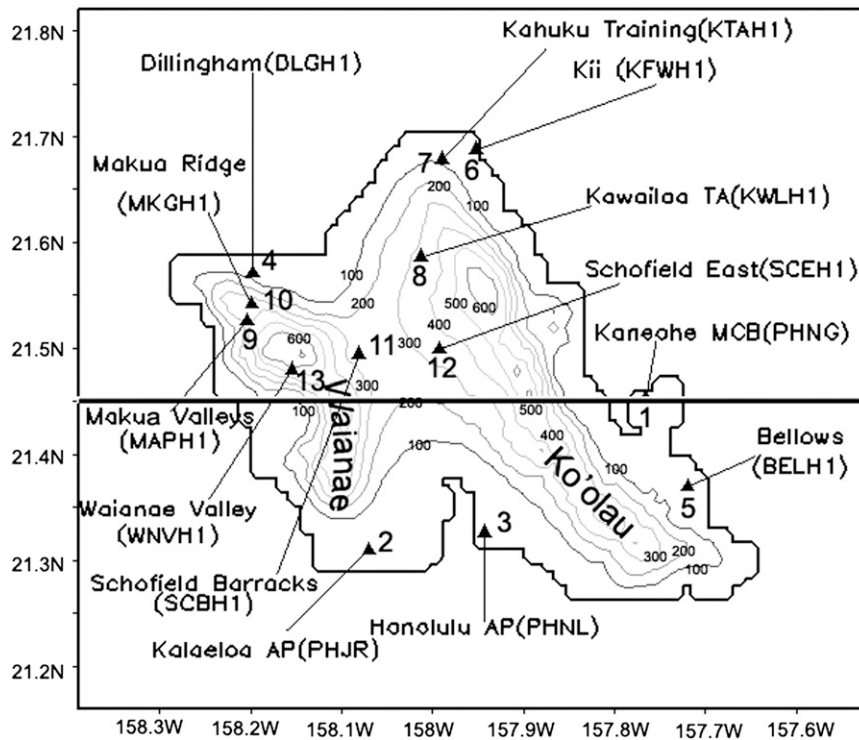


FIG. 2. Locations of 13 hourly weather stations on Oahu, including model terrain height (m) and location of vertical cross sections (21.45°N).

Dudhia radiation scheme (Dudhia 1989). The cumulus parameterization scheme is not used for the 1.5-km Oahu domain.

The GFS output is used to initialize the daily 36-h runs. Sea surface temperature (SST) is updated at the time of initialization from the National Centers for Environmental Prediction (NCEP) SST analysis. An advanced land surface model (Chen and Dudhia 2001) is employed using the vegetation cover and soil properties compiled by Zhang et al. (2005a). Soil moisture and soil temperature input for the LSM are spun up for two months prior to the simulation period (Yang et al. 2005) with the updated soil moisture and soil temperature. The 24-h forecasts of the soil moisture and soil temperature of the previous day are used to update the initial conditions for the model for the following day's simulation. The simulations are performed for a 2-month period: 1 July–31 August 2005. The 24-h model forecast, from the 12th to the 35th hour, is used as the simulated diurnal cycle for each day.

3. Data and analysis method

The 13 hourly surface weather stations and 69 rain gauge stations over Oahu provided observations for model evaluation. The hourly data at the Oahu stations (Fig. 2) include wind speed, wind direction, air temperature, and

dewpoint. The instrument platforms are the Remote Automated Weather Stations (RAWS), Marine Weather Transmitters (MWT), and Automated Surface Observing System (ASOS). Rainfall data used in this study came from the NWS Hydronet, the National Climate Data Center (NCDC) stations, RAWS, ASOS, and the U.S. Geological Survey (USGS). During the summer, trade winds are persistent over the Hawaiian Islands, with a maximum of a 93% chance of occurrence during August (Schroeder 1993). The surface data collected during July–August 2005 are used to validate the model results. The u - and v -wind components, surface air temperature, and dewpoint at the 13 hourly stations were compared to a simple distance-weighted interpolation of the gridded model values to compute model error statistics at the station locations.

To study the effects of terrain and the diurnal heating cycle on island airflow and weather, model simulations are averaged for the two-month period. The spatial distributions and diurnal variations of mean surface wind speed, wind direction, surface air temperature, moisture, and rainfall are examined to study the island effects on airflow and weather. In addition, vertical cross sections of winds, vertical motion, and thermodynamic variables along 21.45°N are constructed for the mean flow as well as for different times during the diurnal cycle. The model

results are used to diagnose the physical processes responsible for the observed diurnal variations of rainfall over the island and the effects of land surface forcing on downslope winds above the leeward slopes of the mountains.

To address the relative importance of daytime heating and orographic blocking on the development of frequently observed westerly reversed flow along the Waianae coast (HC) and the effects of terrain on rainfall production for Oahu, model sensitivity tests are performed for a typical trade wind day on 9 August 2005. The analysis 10-m wind speed at 0000 UTC 9 August for an upstream point (21°N, 152°W) is 7.3 m s^{-1} and the wind direction is 92°. The land-use properties were unchanged in these sensitivity tests.

4. Simulation of the mean state

Observations during 62 days of July and August 2005 are used to validate the model simulations. Model results are also used to study the orographic effects on mean spatial distributions of surface thermodynamic fields, airflow, and rainfall. The simulated fields over Oahu are compared with those at the same height level of an upstream reference point (21.67°N, 157.71°W) over the open ocean.

a. Thermodynamic fields

The error statistics for surface air temperature for July–August 2005 are shown (see Table 1). The root-mean-square error (RMSE) and mean absolute error (MAE) values vary from 1.0 to 2.2 K and from 0.7 to 1.7 K, respectively. The magnitude of both RMSE and MAE are comparable with Yang et al. (2005) for the island of Hawaii. The errors at windward stations are smaller than those at other locations. All MAE values at three windward stations (stations 1, 6, and 7) of the Ko'olau Mountains are relatively small ($<1.1 \text{ K}$). The error statistics of dewpoint at 11 stations (dewpoint observations are not available at Bellows and Kii; Table 1) show that the errors are relatively small at coastal stations (station 1, 2, 3, and 4), and larger at stations (stations 10, 11, and 13) over the Waianae Mountains.

Spatial distributions of simulated mean temperature anomalies from the upstream point at the same height during the two summer months in 2005 are shown in Fig. 3a. Positive anomalies are found downstream of the ridge tops of the Ko'olau Mountains with the largest anomalies ($>1.5 \text{ K}$) in the leeward side of the Waianae Mountains. Secondary positive anomaly maxima were found along the south shore and central Oahu. Both areas are in the lee side of the Ko'olau Mountains. Small negative

temperature anomalies are found along the windward slopes of the Ko'olau Mountains.

The simulated mean mixing ratio anomalies (Fig. 3b) for the two summer months show that the surface air is relatively moist over the windward side of Oahu with a maximum positive anomaly axis ($>0.5 \text{ g kg}^{-1}$) on the windward slopes of the Ko'olau Mountains and an area of minimum anomalies along the western leeward coast ($<-1 \text{ g kg}^{-1}$). The slightly cooler and moist conditions over the Ko'olau Mountains is apparently related to orographic lifting, cloud, and precipitation as the warm, moisture-laden trade wind air is forced up the Ko'olau Mountains. With the removal of moisture by precipitation and sinking motion in the lee, the air is relatively dry and warm downstream of the Ko'olau Mountains. Significant drying and warming occur in the lee side of the Waianae Mountains as well. Over the windward coast, the temperature and moisture anomalies are rather small because of oceanic influences. The maximum positive temperature anomalies occur in the lee side of the Waianae Range and along the south shore, due to adiabatic warming of descending air, and the land surface properties of leeward Oahu.

b. Surface winds

A comparison of the mean observed and simulated winds at the 13 Oahu weather station locations (Fig. 4) showed that the model had the most difficulty representing mean winds at 4 stations in the northern Waianae Range, in the vicinity of Oahu's tallest peak, Mount Ka'ala ($>1200 \text{ m}$). There the model overestimated wind speed and made the largest errors in wind direction. Wind direction errors are relatively small at windward stations. The observed mean wind speeds at the northern Waianae stations were relatively weak. The airflow there is sensitive to the diurnal heating cycle (Table 1 and Fig. 4). Even with a 1.5-km-high horizontal resolution, the model may not be adequate to depict the steep terrain of the Waianae Mountains in sufficient detail (Fig. 2). Although the distance between the Makua Ridge and Makua Valley is small, there are large observed differences in wind direction between these stations, reflecting the differential influences of terrain and proximity to the ocean.

At the surface, the flow decelerates as it approaches the island because of orographic blocking and surface friction. On the windward side of the Ko'olau Mountains, wind speed has a minimum on the windward slopes ($<4 \text{ m s}^{-1}$ versus $6\text{--}8 \text{ m s}^{-1}$ over the open ocean; Fig. 5). The lowest mean wind speed ($<2 \text{ m s}^{-1}$) is simulated over central Oahu extending from the leeward foothills of the Ko'olau Mountains to the windward slopes of the Waianae Mountains. At Schofield Barracks (station 11) in

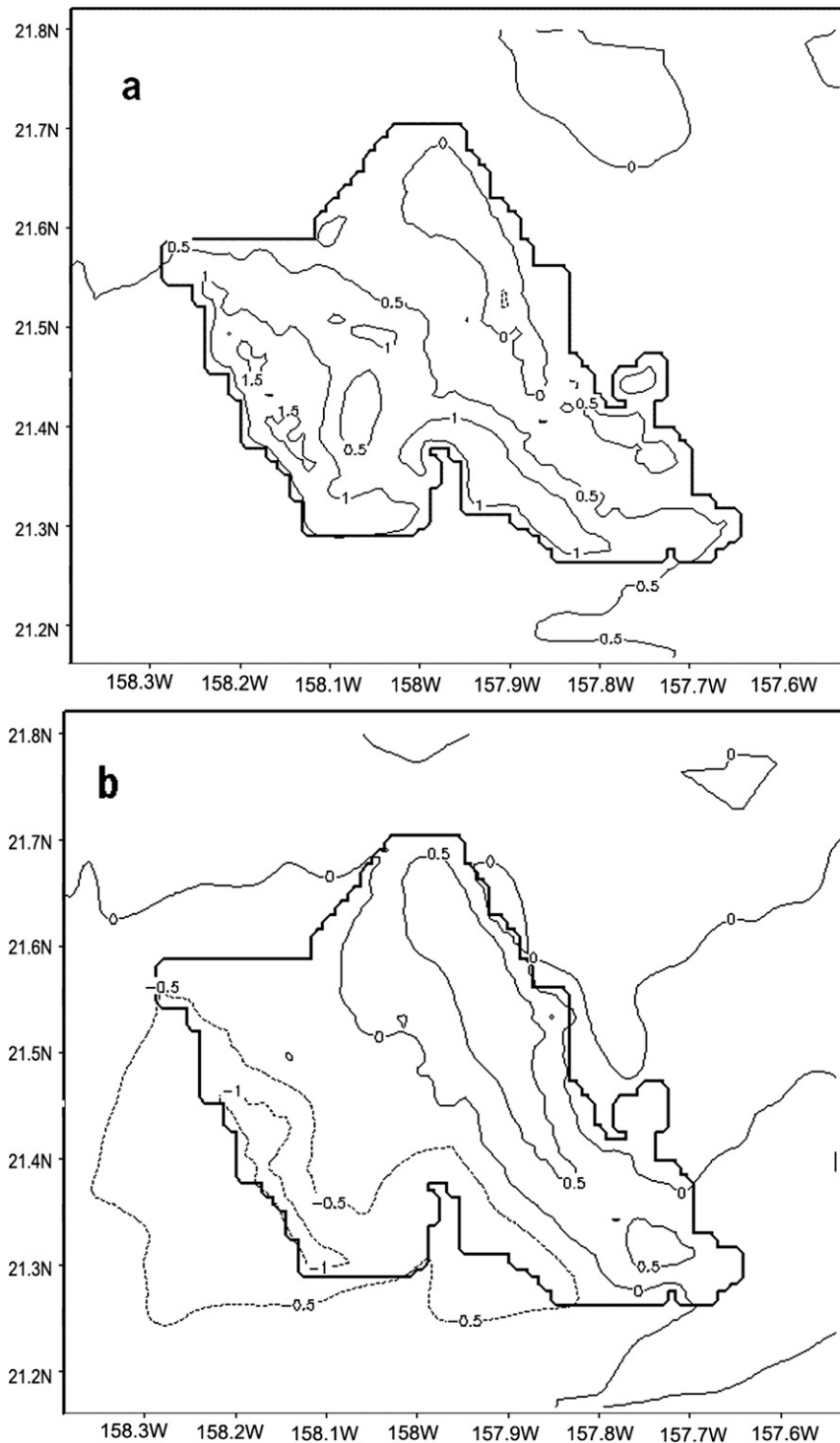


FIG. 3. Mean anomalies from an upstream point (21.67°N, 157.71°W) for the same height during July–August 2005 for (a) 2-m air temperature (K) and (b) mixing ratio (g kg^{-1}).

central Oahu, the simulated mean wind speeds are less than 1 m s^{-1} . Another simulated low wind speed region occurs along the leeward Waianae coast ($<4 \text{ m s}^{-1}$) with local speed minima of $<2 \text{ m s}^{-1}$. Regions off the coast

of the northwestern and southeastern corners of Oahu have wind speeds exceeding 8 m s^{-1} . These winds are stronger than the general trade wind flow over the open ocean ($6\text{--}8 \text{ m s}^{-1}$) because of channeling airflow around

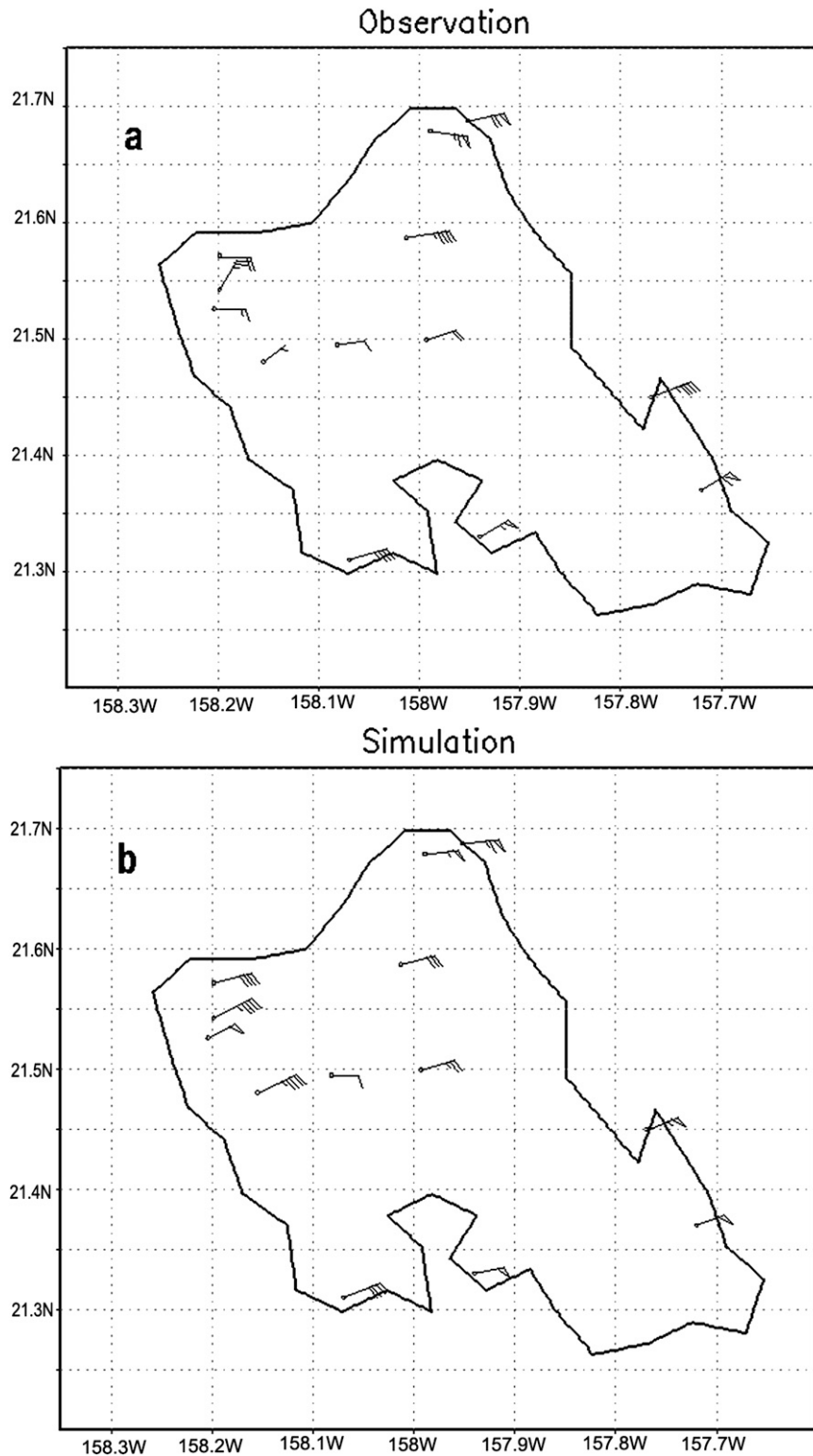


FIG. 4. Mean surface winds (m s^{-1}) during the two summer months based on (a) observation and (b) simulation at 13 weather stations: one pennant is 5 m s^{-1} , full barb is 1 m s^{-1} , and half barb is 0.5 m s^{-1} .

TABLE 1. Error statistics for 13 hourly weather stations.

Station No.	T ($^{\circ}\text{C}$)			T_d ($^{\circ}\text{C}$)			u (m s^{-1})			v (m s^{-1})		
	BIAS	RMSE	MAE	BIAS	RMSE	MAE	BIAS	RMSE	MAE	BIAS	RMSE	MAE
1	-0.1	1	0.7	0.6	1.1	0.9	-1.1	2.2	1.5	-0.4	1.9	1.2
2	1.3	2.1	1.7	0.5	1.5	1.2	-0.5	1.8	1.4	-0.5	1.6	1.2
3	-0.3	1.4	1	1	1.5	1.2	-0.3	2.4	1.9	1.7	2.5	2
4	-0.1	2.2	1.7	0.5	1.6	1.3	-1.9	2.5	2.1	-1.2	2	1.7
5	N/A	N/A	N/A	N/A	N/A	N/A	0.4	1.4	1.1	1.4	2	1.7
6	-1	1.4	1.1	N/A	N/A	N/A	0.5	1.6	1.2	0.8	1.8	1.4
7	-0.8	1.5	1.1	-2.6	2.8	2.6	1	1.8	1.4	-1.6	2.1	1.7
8	-0.1	1.9	1.5	0.9	2.1	1.3	1.2	2.9	2.2	-0.1	1.3	1
9	-1.1	2	1.5	-0.6	1.7	1.4	-3.1	4	3.4	-2.3	3	2.5
10	0	1.5	1.1	-1	1.9	1.4	-2.8	3.5	2.9	0.3	2.4	1.9
11	-0.1	1.7	1.3	1.2	2	1.6	0.3	1.8	1.5	0.2	1.6	1.3
12	0.8	1.9	1.4	0.2	1.6	1.3	-0.4	2.9	2.3	0	1.7	1.3
13	-1.2	2	1.6	-2.5	3.1	2.6	-3.8	4.7	4	-1.6	3.2	2.6
All	-0.1	1.8	1.4	-0.1	2	1.5	-0.8	2.8	2.1	-0.2	2.2	1.7

the corners of the island, consistent with previous observational studies (Leopold 1948; Ramage and Oshiro 1977).

c. Rainfall

There are large spatial variations in the simulated rainfall accumulation during the 62-day period of study. Simulated rainfall accumulation has a maximum over the Ko'olau Mountains, a secondary maximum over the Waianae Mountains, and a minimum over central Oahu, in agreement with observations (Fig. 6). The model overestimates rainfall over both mountains, especially on the windward side of the Ko'olau Mountains. With a relatively narrow ridge axis, the orographic precipitation on the windward side of the Ko'olau Mountains can spread to the western leeside slopes, as clouds and liquid water are carried by the prevailing winds. This feature may not be well captured by the model.

Even though the Waianae Mountains are steeper and higher than the Ko'olau Mountains, both the observed and simulated rainfall accumulations are much less than over the Ko'olau Mountains. The Waianae Mountains are downstream of the Ko'olau Mountains with much weaker winds impinging upon them (Fig. 5) as compared with the upstream trade wind flow. Furthermore, the air that impinges on the Waianae Mountains is drier than the trade wind flow over the open ocean (Fig. 3b) as a part of the moisture in the flow from over the ocean is depleted by orographic precipitation over the Ko'olau Mountains.

5. Diurnal regimes

a. Simulated thermodynamic fields for the daytime and nighttime regimes

The simulated surface air temperatures at 1400 HST agree with observations reasonably well. Both RMSE

and MAE values at windward stations (stations 1, 6, and 7) are smaller than other stations (Table 2). The simulated surface air temperatures match observations better at 0500 than at 1400 HST, except at the two leeward coastal stations (stations 2 and 4). All three windward stations (stations 1, 6, and 7) have MAE less than 1 K at 0500 HST; all other stations, except stations 2 and 4, have MAE less than 1.5 K (Table 2).

The simulations of dewpoint at 1400 HST are in reasonable agreement for most stations except station 7 at the northern end of the Ko'olau Mountains and station 13 in Makua Valley on the leeside of the Waianae Mountains (Table 2). Errors for both stations could be related to the influence of the sea breezes and the fact that the complex terrain there may not be properly resolved by the 1.5-km grid. The error statistics for dewpoint at 0500 HST are better than at 1400 HST, with MAE less than 1.6 K for all stations except station 7.

Along the portion of the windward coast that is well exposed to the incoming trade wind flow, temperature anomalies deviating from the open-ocean value at the same height at 1400 HST are smaller than 1 K (Fig. 7a). This is in contrast to the island of Hawaii, which is dominated by the massive Mauna Loa and Mauna Kea Mountains and a relatively large island size (~ 140 km). The daytime temperature anomalies reach 2–3 K along the windward coast of the island of Hawaii (Chen and Wang 1994). The Oahu temperature anomalies are lower on the windward side of the Ko'olau Mountains and higher on the lee sides of both the Ko'olau Mountains and the Waianae Mountains with descending airflow (section 5c). There are three local temperature anomaly maxima on the lee sides of the mountains (>6 K): over central Oahu, the urban areas of Honolulu along the southern coast, and in the central leeside of the Waianae Mountains. The positive temperature anomalies in those

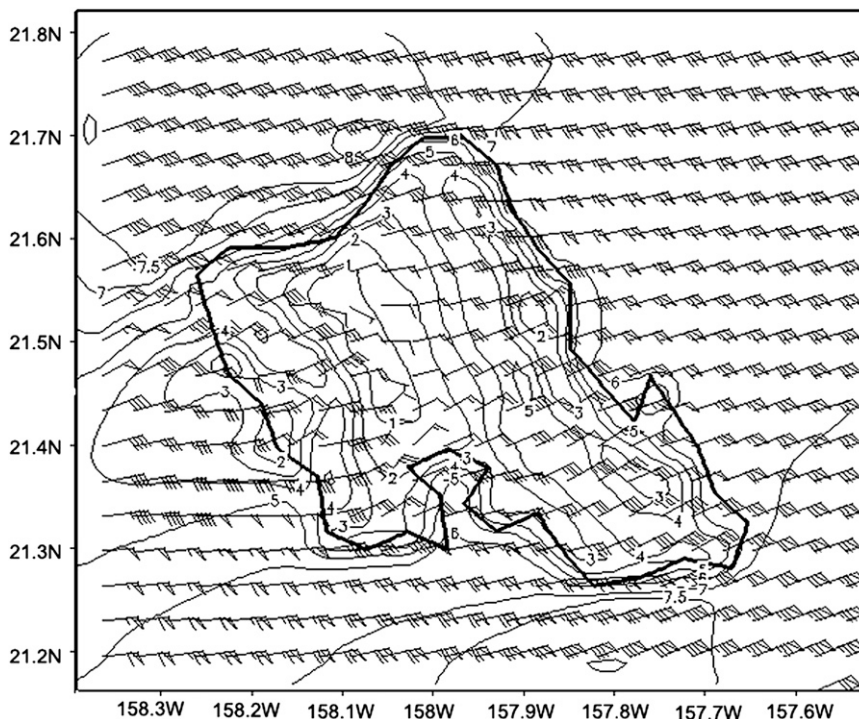


FIG. 5. As in Fig. 4, but for the simulated horizontal distribution of surface winds and isotachs every 1 m s^{-1} .

leeside areas are comparable to the leeside areas of the island of Hawaii where the ridges and mountaintops lie below the typical height of the trade wind inversion ($\sim 2 \text{ km}$). Both areas experience similar descending airflow in the lee (section 5c) as well as latent heat release due to orographic precipitation on the windward side and over the ridge tops of the mountains. The temperature anomalies on the windward side and over the ridge tops of the Ko'olau Mountains (2–3 K) are lower than those areas over the Waianae Mountains (4–5 K) because of dense cloud cover (Fig. 7b) and frequent orographic rain on the windward slopes and ridge tops of the Ko'olau Mountains in the afternoon. The orographic precipitation over the Waianae Mountains is much less than that over the Ko'olau Mountains because of the rain shadow effect (HC). Furthermore, the differences in land-use categories between the two mountains also contribute to the temperature differences. Over the Ko'olau Mountains, the dominant ground cover is tropical rain forest with a large vegetation fraction (close to 100%), whereas the dominant land categories over the Waianae Mountains are grassland, scrubland, and pasture. The skin surface temperature at 1400 HST (Fig. 7c) is closely related to variations in ground cover. It is apparent that early afternoon temperature anomalies over Oahu (Fig. 7a) are related to airflow, daytime heating of

different land-use types, and distributions of clouds and rain.

With a relatively small island size and lower terrain heights as compared with the island of Hawaii, the negative temperature anomalies over Oahu at night (-0.5 to -1.5 K ; Fig. 7d) are smaller than those over the Big Island (-2 to -3 K ; Chen and Wang 1994). The largest negative temperature anomalies ($< -1.5 \text{ K}$) occur over central Oahu between the Ko'olau Mountains and the Waianae Mountains (Fig. 7d) because of the weak drainage flow coming down from the eastern lower slopes and foothills of the Waianae Mountains (section 5b). Along the windward coast, the surface temperature is comparable to the upstream values. In contrast, over the Hilo Bay area of the island of Hawaii, the negative temperature anomalies are lower than -3 K (Chen and Wang 1994) as the katabatic flow on the windward lower slopes moves down the slopes and accumulates along the coast (Feng and Chen 1998). The negative temperature anomalies are relatively small along the ridgeline of the Ko'olau Mountains ($> -0.5 \text{ K}$) because of orographic cloud cover (Fig. 7e). In the lee sides of the Waianae Mountains and southeastern arm of the Ko'olau Mountains, with their relatively steep and narrow mountain ridges, the negative temperature anomalies are the smallest because of the descending airflow in the lee.

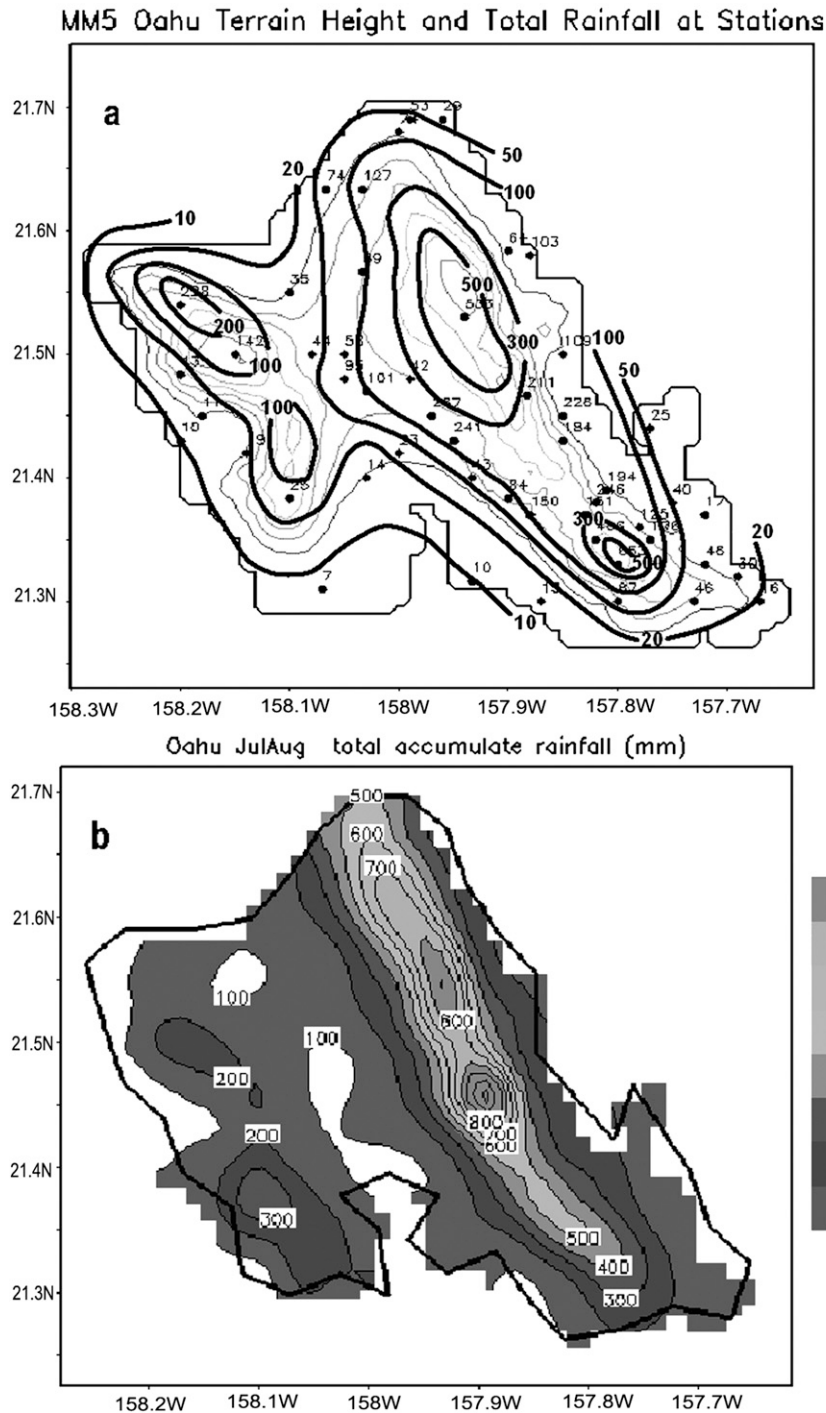


FIG. 6. Total rainfall accumulation (mm) during July–August 2005 based on (a) analysis from surface observations, model terrain in light contours (every 100 m), and (b) the simulation (every 100 mm).

During the daytime, a moist axis ($>0.5 \text{ g kg}^{-1}$) is simulated on the windward slopes of the Ko'olau Mountains as a result of orographic lifting with relatively dry conditions downstream. The driest areas ($<-1.5 \text{ g kg}^{-1}$)

are along the southern coast in urban Honolulu and along the leeside of the Waianae coast (Fig. 8a) as a result of the combined effects of descending flow in the lee and daytime vertical mixing (section 5c). At night,

TABLE 2. Error statistics for T and Td at 0500 and 1400 HST.

Station No.	0500 HST (T °C)			0500 HST (Td °C)			1400 HST (T °C)			1400 HST (Td °C)		
	BIAS	RMSE	MAE	BIAS	RMSE	MAE	BIAS	RMSE	MAE	BIAS	RMSE	MAE
1	0.2	0.9	0.6	1.1	1.4	1.1	0	1.3	0.9	0.2	0.9	0.7
2	2.6	2.8	2.6	1.4	1.7	1.5	1.6	2.5	2.1	-0.5	1.5	1.1
3	-0.1	1	0.8	1.3	1.7	1.4	0.3	2	1.6	0.8	1.5	1.2
4	2.2	2.9	2.4	1.5	1.9	1.6	-0.7	2.2	1.7	-0.2	1.6	1.3
5	N/A	N/A	N/A	N/A	N/A	N/A	N/A	N/A	N/A	N/A	N/A	N/A
6	-0.5	1.1	0.8	N/A	N/A	N/A	-1.3	1.6	1.4	N/A	N/A	N/A
7	-0.3	1.1	0.9	-2.3	2.4	2.3	-1.2	2	1.5	-3.1	3.3	3.1
8	-1.3	1.7	1.5	1.4	1.7	1.5	1.8	2.8	2.4	0.1	1.2	1
9	-0.4	1.3	1.1	0.4	1.2	0.9	-1.4	2.8	2.3	-1.8	2.5	2.1
10	0.1	0.8	0.6	-0.1	1	0.7	0.1	2.4	1.9	-2.1	2.6	2.2
11	1.1	1.6	1.3	1.2	1.8	1.4	-0.5	2	1.4	1	1.7	1.4
12	0.3	1.3	1	1.3	1.8	1.5	1.9	2.9	2.4	-1.1	1.8	1.5
13	-0.9	1.5	1.3	-1.2	1.6	1.4	-2.2	3	2.4	-4.4	4.6	4.4
All	0.6	1.9	1.4	0.8	1.8	1.5	0	2.3	1.8	-0.7	2.3	1.8

a moist axis ($>0.5 \text{ g kg}^{-1}$) is simulated over the Ko'olau Mountains due to orographic lifting and rain evaporation. The moist conditions extend to the lee side, especially over the southeastern areas of the Ko'olau Mountains where nocturnal showers encounter a relatively narrow mountain ridge (Fig. 8b). The driest area at night is simulated along the Waianae leeside coast ($<-0.5 \text{ g kg}^{-1}$). The south shore is also relatively dry.

b. Simulated daytime and nighttime flow regimes

Both the wind speed and wind direction change considerably during the diurnal cycle. Along the windward coast, the decrease in wind speed from the open-ocean value ($6-8 \text{ m s}^{-1}$) during the day is less significant than at night, in agreement with observations (Fig. 9). The simulated wind speed along the windward coast during the day is about $5-6 \text{ m s}^{-1}$ as compared with $4-5 \text{ m s}^{-1}$ at night. At night, with cooler air over the island, the simulated flow deceleration on the windward side is more significant with a wind speed minimum $\sim 1-2 \text{ m s}^{-1}$ at the foothills as compared to $\sim 2-4 \text{ m s}^{-1}$ during the day (Fig. 10). In contrast, both the observed and simulated wind speeds over the island interior west of the Ko'olau Mountains are stronger during the daytime (Figs. 9c,d) because of vertical mixing of trade wind momentum (Leopold 1948; Zhang et al. 2005a) than at night (Figs. 9a,b; 3-4 versus $1-2 \text{ m s}^{-1}$; Fig. 10).

At 0500 HST, the winds over central Oahu are calm with relatively weak winds over the island interior (Fig. 10a). The observed weak katabatic winds were simulated on the eastern slopes of the Waianae Mountains. In the afternoon, the observed combined upslope/trade wind flow develops on the eastern slopes of the Waianae Mountains in the model (Fig. 10b).

Along the central Waianae coast, the downslope/offshore flow dominates at night. The observed onshore

flow along the central Waianae coast in the afternoon hours is reproduced in the model. The relative role of thermal forcing versus orographic blocking in the production of westerly reversed flow off the leeside coast during the daytime will be investigated in section 7 from model sensitivity tests.

c. Simulated winds aloft

Vertical cross sections of mean zonal wind components along 21.45°N (Fig. 2) at 0500 and 1400 HST are constructed to investigate winds aloft for both the daytime and nighttime flow regimes. The location 21.45°N is selected because the vertical cross sections at this latitude can capture the onshore/sea-breeze flow over the leeside of the Waianae Mountains during the day, the weak wind areas over central Oahu, and the strong downslope winds on the leeside slopes of both mountain ranges at night. In this section, we will show that, in addition to surface airflow, the airflow aloft is also strongly modulated by the daytime heating and nighttime cooling.

At night, strong downslope winds ($>10 \text{ m s}^{-1}$) above the leeside slopes of both the Ko'olau and the Waianae Mountains were simulated (Fig. 11a). The simulated wind speeds aloft over the leeside slopes are about 40% stronger than over the open ocean. These areas are the locations that experience high winds under strong trade wind conditions (Zhang et al. 2005b). On the windward slopes, the low-level potentially cooler air is forced upward by orographic lifting whereas on the leeside slopes, the potentially warmer air aloft is brought downward by the strong downslope winds (Fig. 11a). Except within the thin katabatic flow layer on the windward slopes of the Waianae Mountains, the contour lines of the equivalent potential temperature tilt upward on the windward sides of both mountains (Fig. 12a). On the leeside slopes, strong descending flow with downward tilt of the equivalent

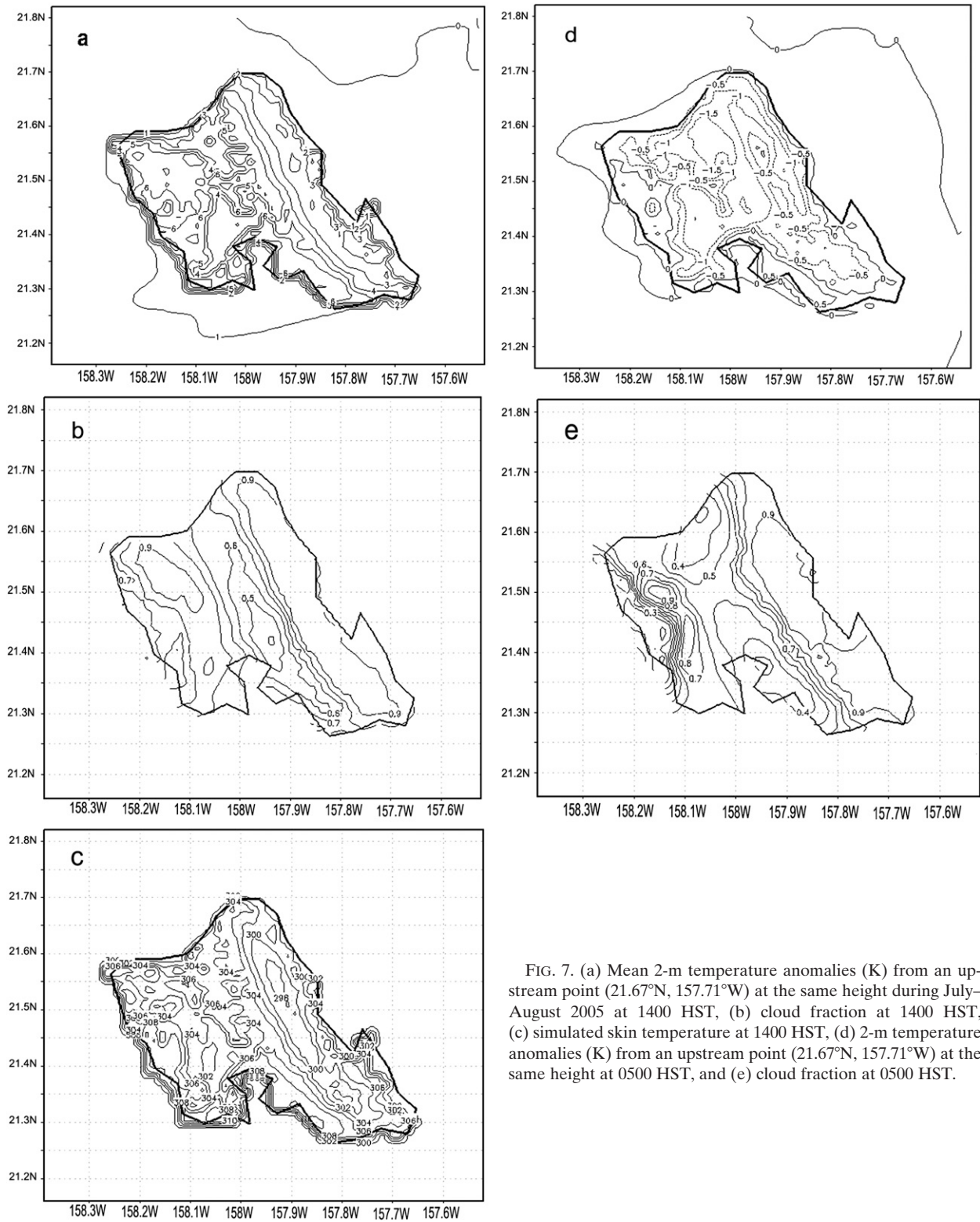


FIG. 7. (a) Mean 2-m temperature anomalies (K) from an upstream point (21.67°N, 157.71°W) at the same height during July–August 2005 at 1400 HST, (b) cloud fraction at 1400 HST, (c) simulated skin temperature at 1400 HST, (d) 2-m temperature anomalies (K) from an upstream point (21.67°N, 157.71°W) at the same height at 0500 HST, and (e) cloud fraction at 0500 HST.

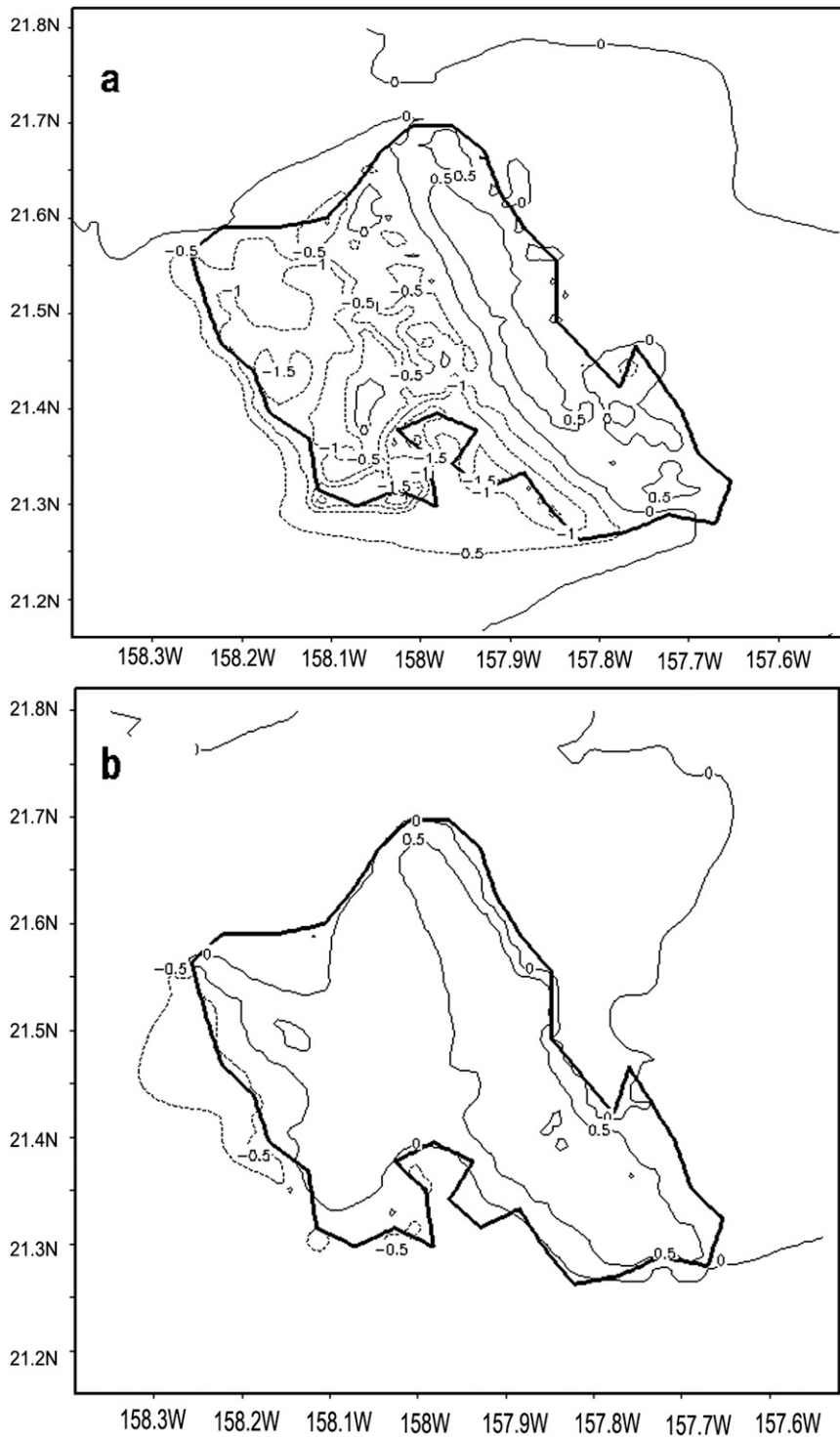


FIG. 8. Mean 2-m mixing ratio anomalies (g kg^{-1}) from an upstream point (21.67°N , 157.71°W) during July–August 2005 at (a) 1400 and (b) 0500 HST.

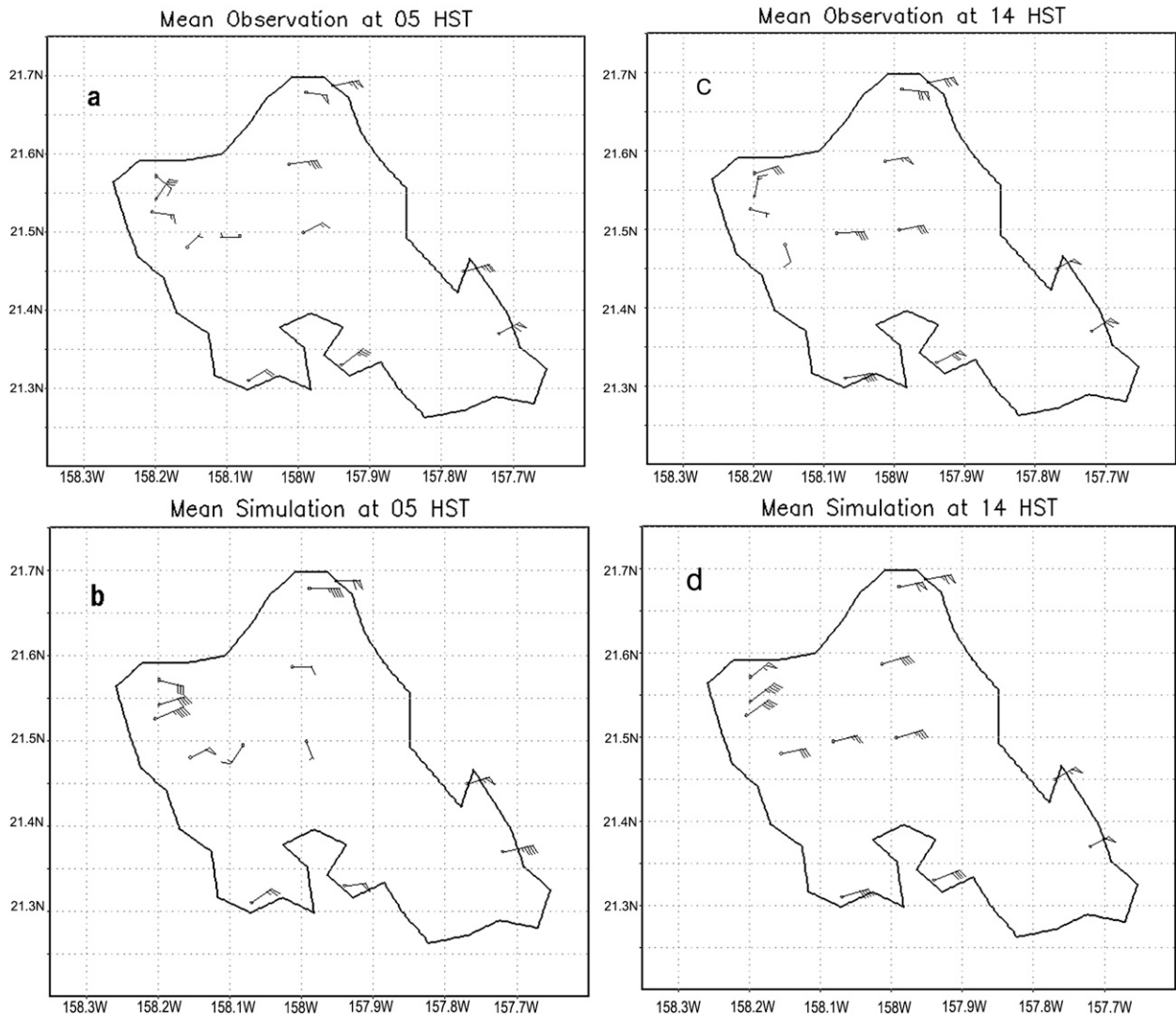


FIG. 9. As in Fig. 4, but for (a) observed and (b) simulated winds at 0500 HST; and for (c) observed and (d) simulated wind at 1400 HST.

potential temperature contours is followed by an upward tilt of the equivalent potential temperature contours (Fig. 12a). With a steeper terrain for the Waianae Mountains than the Koʻolau Mountains, the downslope winds, adiabatic warming, and downward tilt of the equivalent potential temperature contours in the lee of the Waianae Mountains are more significant than over the Koʻolau Mountains (Figs. 11a and 12a).

In the afternoon, with the decrease in stability, increase in vertical mixing in the boundary layer, and lower pressure over land due to solar heating, strong downslope winds were not simulated to the lee of the Waianae Mountains (Figs. 11b and 12b). Only relatively weak descending easterly winds ($\sim 6 \text{ m s}^{-1}$) occurred aloft (Fig. 11b). At the surface, onshore flow develops along the leeside coast of the Waianae Mountains (Fig. 10b).

The simulated downslope winds aloft to the lee of the Koʻolau Mountains are weaker than at night because of the decrease in stability during the day due to land surface heating and vertical mixing (Leopold 1948; Zhang et al. 2005a). At the surface, the simulated nighttime katabatic winds at the foothills and windward slopes of the Waianae Mountains are replaced by the combined daytime upslope/trade wind flow in the model (Fig. 10).

The diurnal variations of U/N at an upstream point (21.67°N , 157.71°W) and over central Oahu (21.45°N , 157.9°W) for the 300–600-m layer above the surface are given in Fig. 13. It is apparent that under normal trade wind conditions, with $U/N > 1.5 \text{ km}$ (Fig. 13a), the air parcels are able to ascend to the mountaintops of the Koʻolau Mountains throughout the diurnal cycle with a large-amplitude gravity wave above the peak (Figs. 11

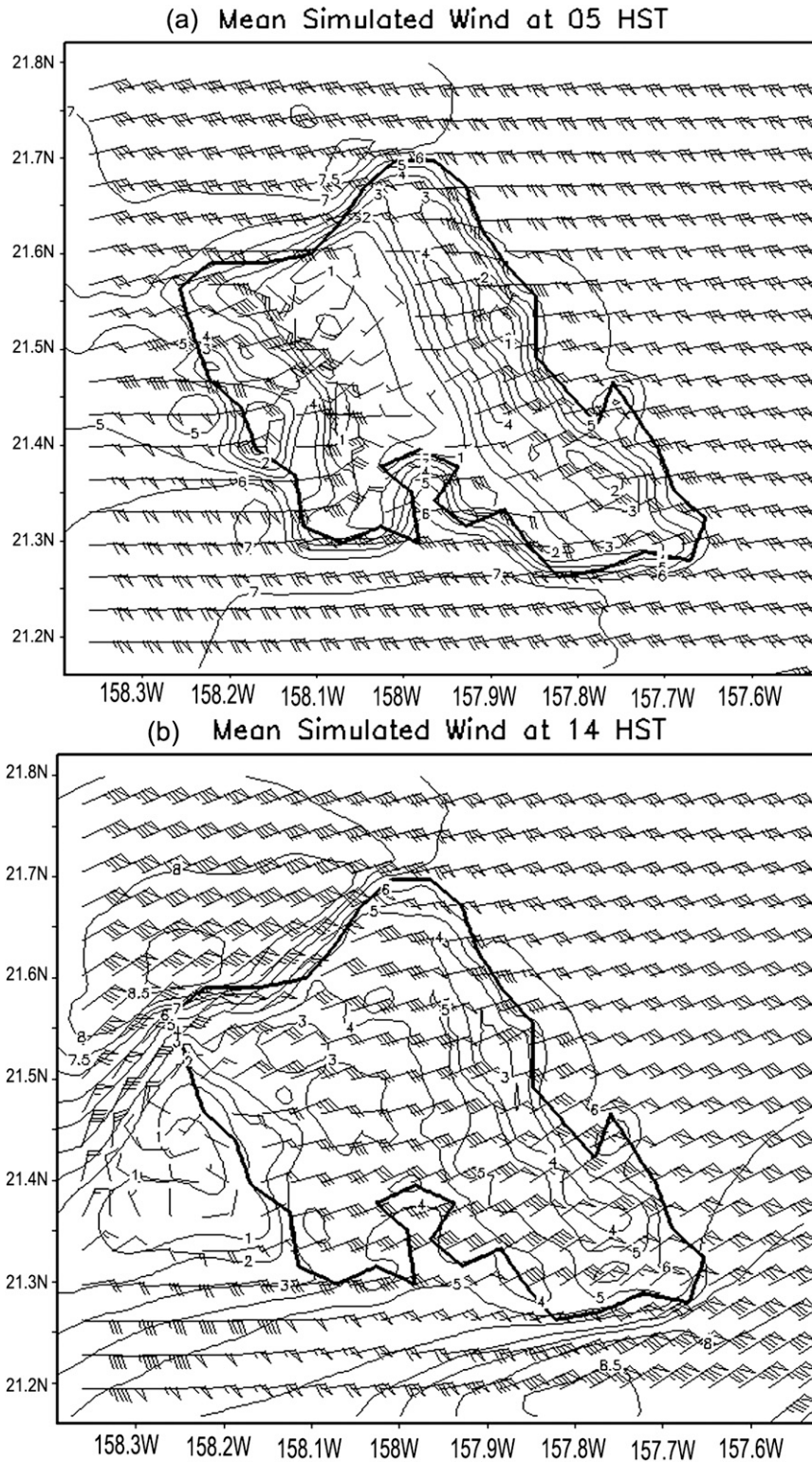


FIG. 10. As in Fig. 5, but for (a) 0500 and (b) 1400 HST.

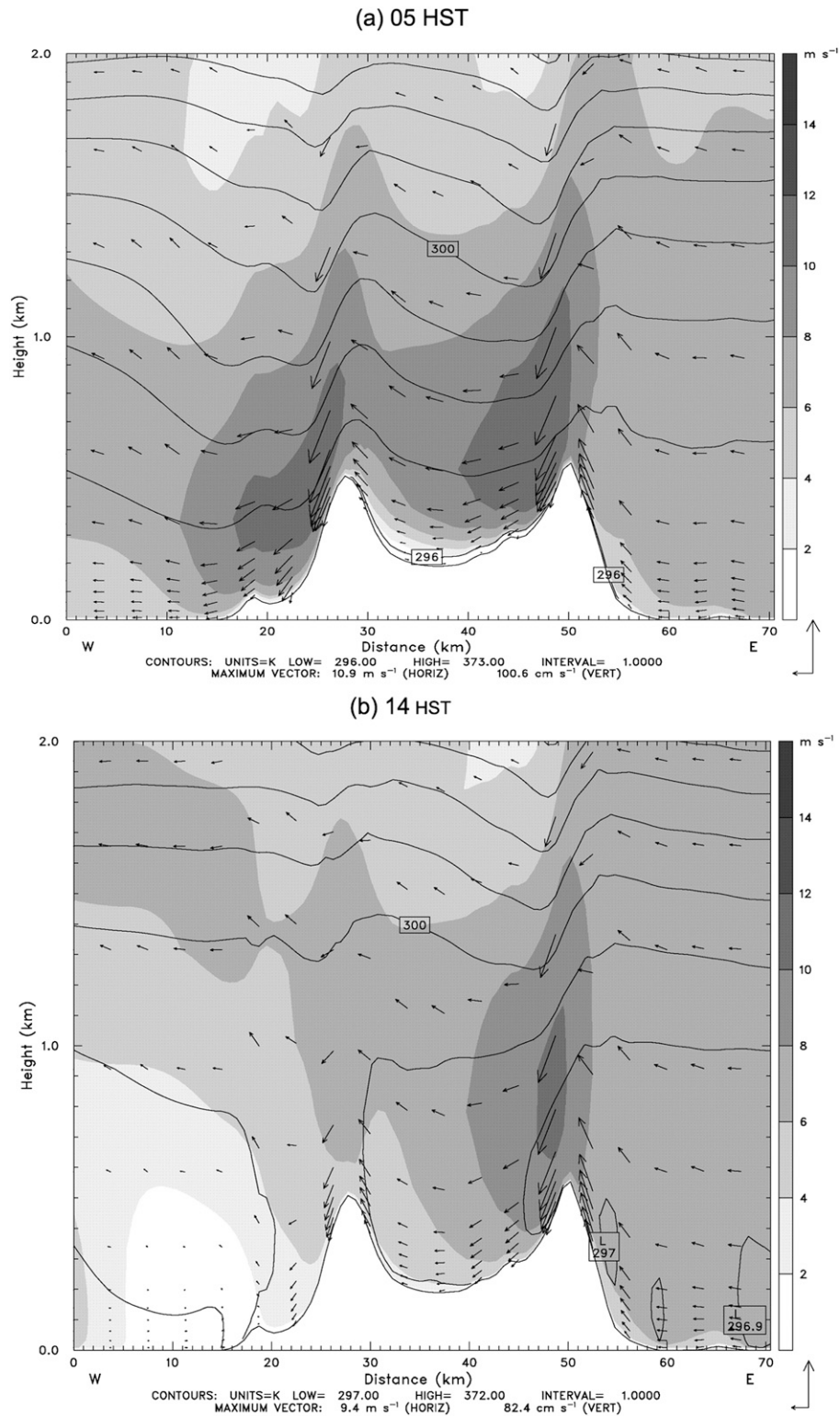
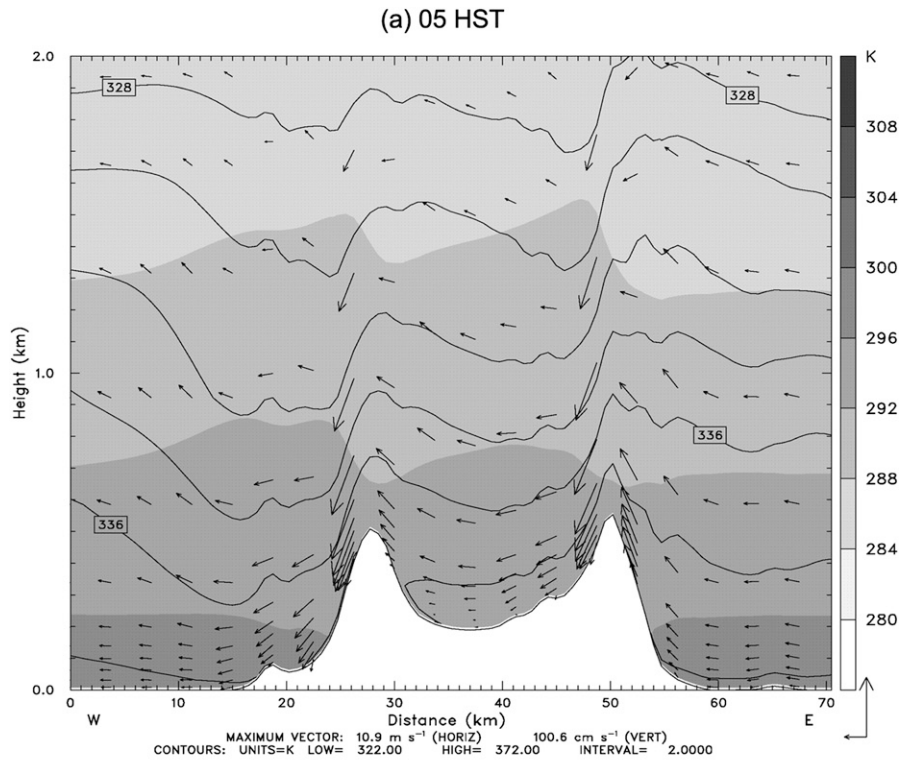


FIG. 11. Vertical cross section at 21.45°N of mean wind speed (shaded, interval: 2 m s⁻¹), mean wind vectors, and potential temperature (contour, interval 1 K) at (a) 0500 and (b) 1400 HST during July–August 2005.



(b) 14 HST

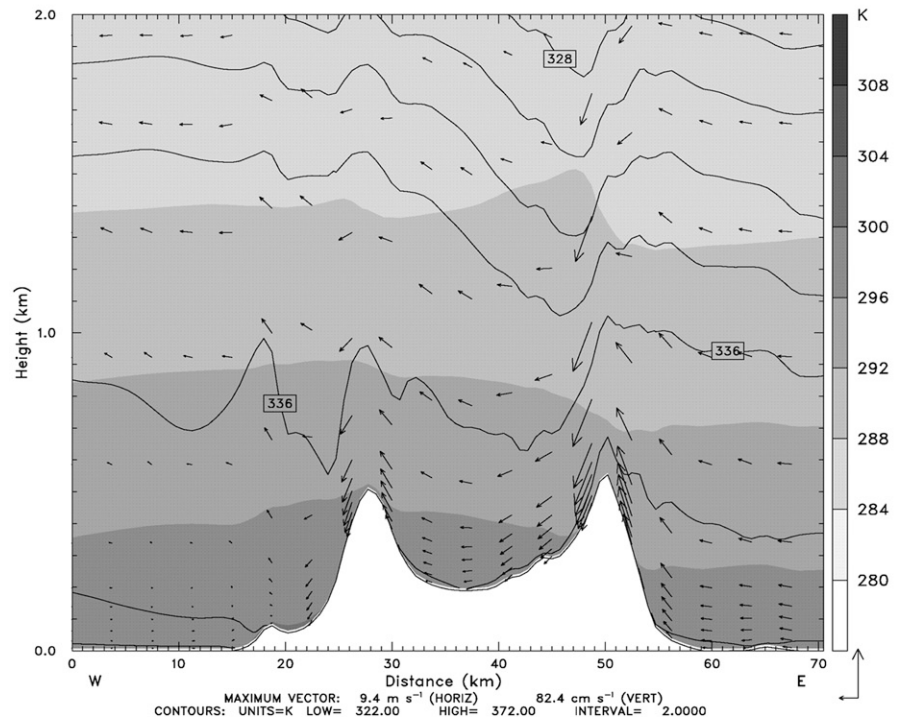


FIG. 12. As in Fig. 11, but the contour is for equivalent potential temperature (K) and the shading is for temperature (K) at (a) 0500 and (b) 1400 HST during July–August 2005.

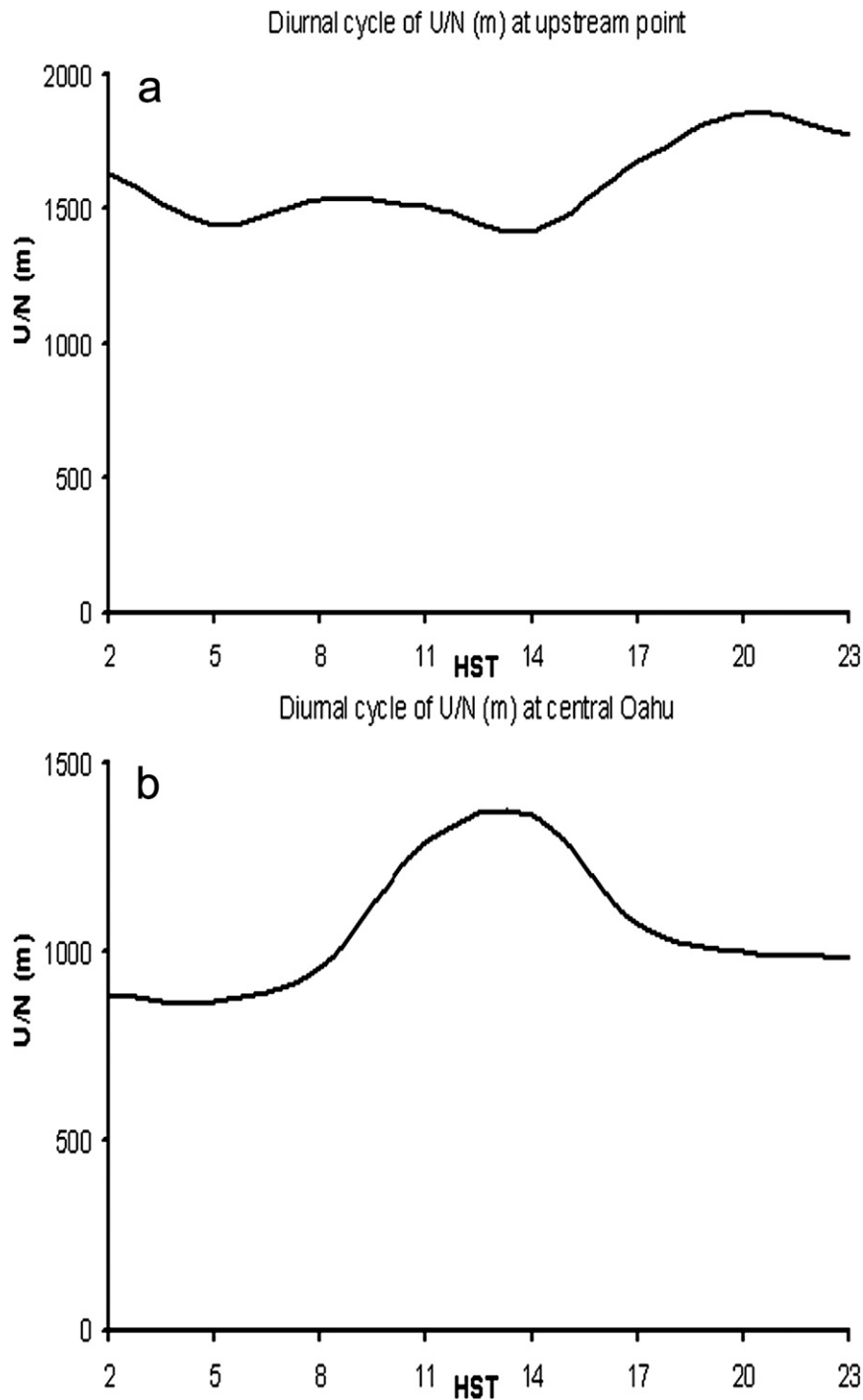


FIG. 13. The diurnal variations of U/N at (a) an upstream point (21.67°N , 157.71°W) and (b) over central Oahu (21.45°N , 157.9°W) for the 300–600-m layer above the surface.

and 12). The largest U/N value in the early evening (>1.8 km) is a reflection of slightly stronger winds aloft at that time. Over central Oahu, U/N has large diurnal variations (Fig. 13b) related to change in stability in response to the diurnal heating cycle. It is apparent that

during the daytime, with the development of the daytime upslope flow on the windward side of the Waianae Mountains, the heated air over central Oahu is able to flow over the tops of the Waianae Mountains. At night, with $U/N \sim 1$ km; and with a ~ 900 -m difference in

elevation between the highest peaks (~1200 m) of the Waianae Mountains and central Oahu (~300 m), the air parcels still can move over the Waianae Mountains except at the lowest levels where cold westerly drainage flow occurs (Fig. 10a).

6. Simulated diurnal rainfall variations

To investigate the diurnal cycle of rainfall, simulations and observations of 3-h rainfall accumulation during the two summer months are averaged to obtain maps of 3-h rainfall accumulations for 2300 to 0200, 0500 to 0800, 1100 to 1400, and 1700 to 2000 HST (Fig. 14). These time periods were selected to capture the early morning rainfall maximum, the secondary rainfall maximum in the early evening, the early afternoon minimum over the Ko'olau Mountains, and the late afternoon rainfall maximum along the western leeward coast (HC). It is notable that the simulated diurnal and spatial variations of rainfall are in good agreement with observations (Fig. 14). The observed nocturnal rainfall over the Ko'olau Mountains, with an early evening maximum and a maximum in the early morning, is well simulated in the model. Along the leeward slopes of the Waianae Mountains, a small amount of rainfall (>1 mm) was simulated in the late afternoon/early evening (from 1700 to 2000 HST), which Leopold (1948) attributed to convective showers as a result of orographic lifting. This occurs when onshore flow brings in warm, moist air from the ocean and moves upslope to produce clouds and possibly light local showers.

Over the Ko'olau Mountains, rainfall is at a minimum during the daytime (Fig. 14). To investigate the causes for the diurnal variations of rainfall over the windward side as well as over the Ko'olau Mountains, 3-h time-height cross sections of simulated meteorological variables at 21.45°N, 157.85°W, along the windward foothills, are constructed (Fig. 15). Figure 15a shows that the simulated low-level equivalent potential temperature is at a minimum around noon as a result of vertical mixing. The simulated vertical motions at 21.45°N, 157.85°W are consistent with the diurnal variations of rainfall. The anomalies of vertical motions from the daily mean at that location exhibit two maxima, at 0800 and 2000 HST, respectively (Fig. 15b). With stronger vertical motions and slightly higher low-level equivalent potential temperature, the simulated rainfall is higher at these times than other time periods during the day.

The simulated easterly wind in the surface layer on the windward side is the weakest before sunrise and strongest in the late afternoon (Fig. 16). The simulated stronger winds in the surface layer during the afternoon give rise to anomalous rising motions in the lowest levels (Fig. 15b).

However, above the surface layer, anomalous sinking motions are present (Fig. 15b) around noontime because of relatively weaker winds aloft (Fig. 15c). With a relatively high lifting condensation level (LCL) and LFC (Fig. 15d), and weaker rising motions, the rainfall has a daily minimum in the early afternoon. Around sunset, the winds aloft strengthen (Fig. 15c). The evening maximum in vertical motion occurs at the time when the wind speed aloft is the strongest. In the early morning, low-level flow deceleration is most significant (Fig. 16) when the land surface is the coolest, giving rise to an early morning maximum in vertical motion (Fig. 15b).

A vertical cross section of airflow is plotted at 21.45°N (Fig. 17). The mean flow shows rising motions along both the windward side of the Ko'olau Mountains and the Waianae Mountains, with descending downslope winds in the lee (Fig. 17a). Note that because of steeper terrain on the windward side of the Ko'olau Mountains, compared with that of the Waianae Mountains, and the effects of latent heat release, the rising motion on the windward slopes of the Ko'olau Mountains, is stronger than along the Waianae Mountains. The persistent orographic lifting on the windward side of the Ko'olau Mountains with descending flow in the lee is consistent with the fact that rains falling on the windward side are generally showers, whereas, after the passage over the barrier, rains falling are relatively light and sometimes continuous (Woodcock 1975). In the early morning, with decelerating airflow on the windward side at low levels, an anomalous rising motion is simulated on the windward foothills with an anomalous sinking motion on the slopes of the Ko'olau Mountains (Fig. 17b).

In the early afternoon, winds aloft over the island are weaker than the mean flow (Fig. 15c) with westerly anomalies and relatively strong surface winds (Fig. 16) as a result of vertical mixing. On the windward slopes of the Ko'olau Mountains and the Waianae Mountains, anomalous rising motion is limited to the surface layer with anomalous sinking motion aloft (Fig. 17c). Over the Waianae leeward slopes, anomalous rising motion develops in the afternoon hours with relatively shallow anomalous westerly winds in low levels (<1 km).

In the early evening, winds aloft strengthen after sunset (Figs. 15c and 17d) with anomalous rising motions on the windward side of both mountains and anomalous descending airflow in the lee (Fig. 17d). The orographic lifting on the windward side and the downslope winds in the lee of both mountains are the strongest in the evening when winds aloft are the strongest. With continued nocturnal cooling throughout the night, low-level winds weaken as orographic blocking on the windward side of the Ko'olau Mountains becomes more significant (Fig. 16).

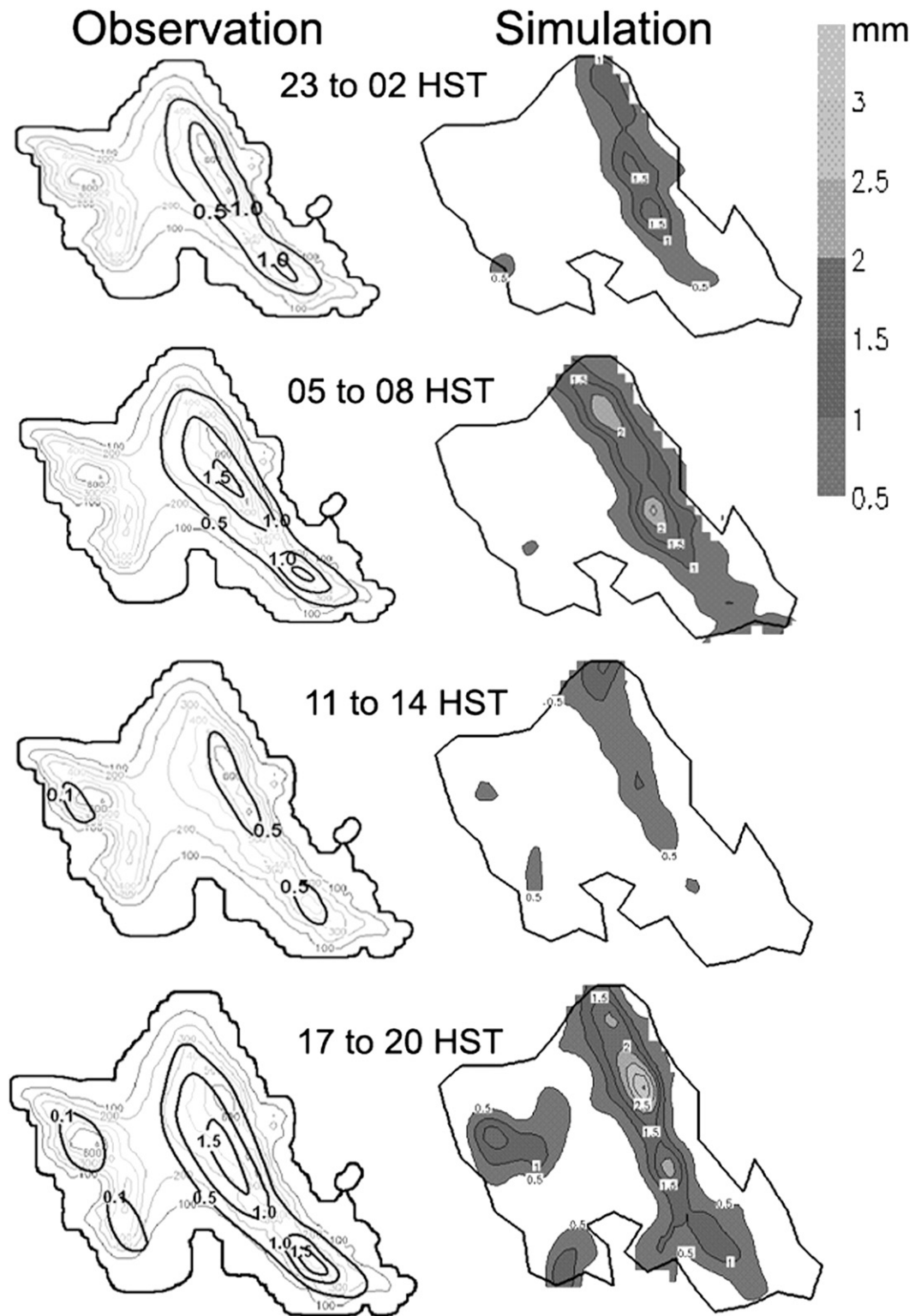


FIG. 14. The 3-h rainfall accumulation during July–August 2005: (left) observed and (right) simulated rainfall (mm).

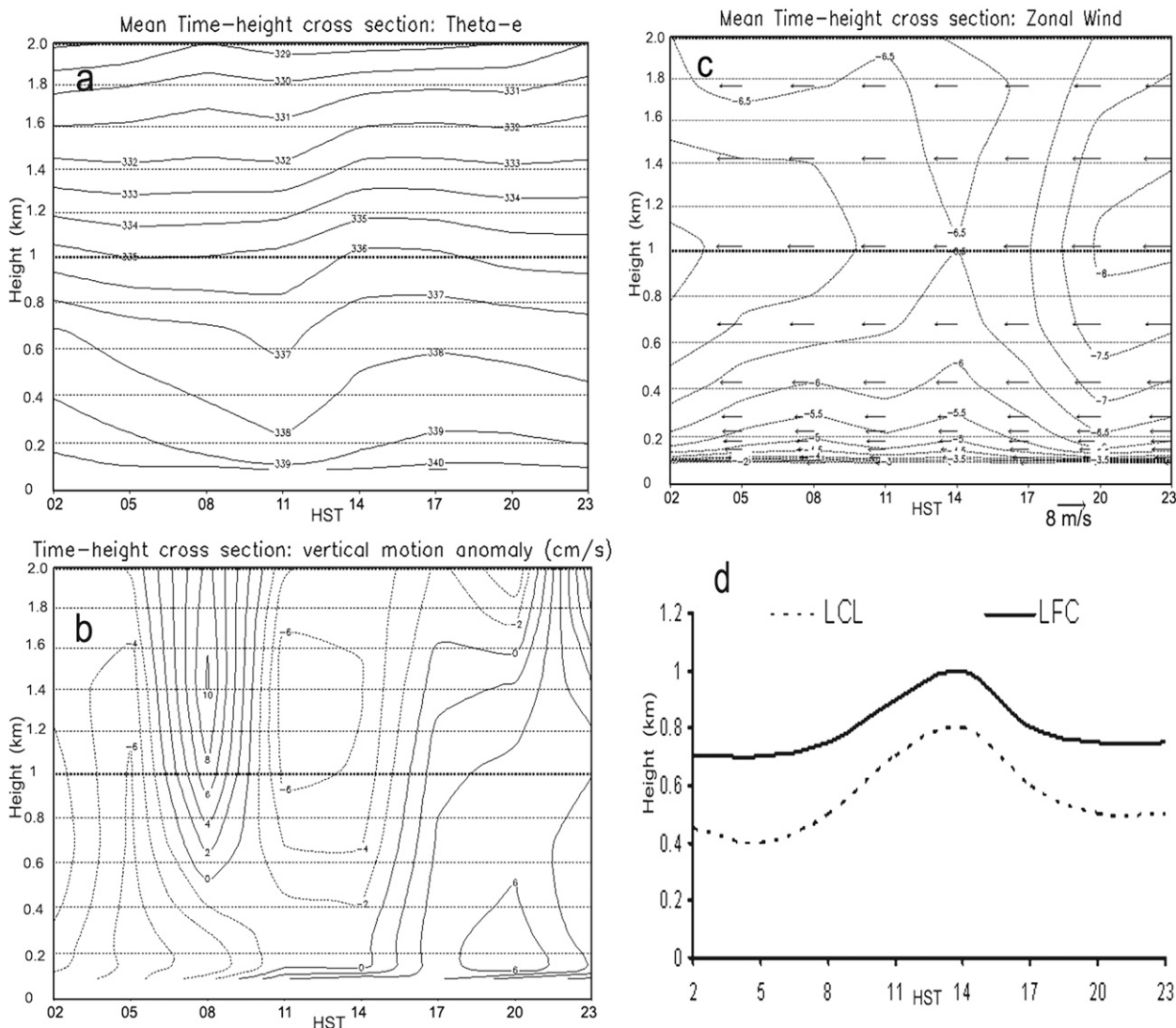


FIG. 15. Time series plots of 3-h simulated meteorological variables at 21.5°N, 157.85°W for (a) equivalent potential temperature (K), (b) deviations of vertical motions from the daily mean (cm s^{-1}), (c) zonal winds (m s^{-1}), and (d) LCL and LFC in km.

It is apparent that the early morning rainfall maximum over the Ko’olau Mountains is related to significant flow deceleration on the windward side, in addition to cloud-top radiation cooling proposed by early studies (e.g., Leopold 1948). The evening rainfall maximum after sunset is related to anomalous orographic lifting due to stronger winds aloft.

7. Mechanisms for the development of westerly reversed flow off the Waianae coast

To investigate the impact of orographic effects on the leeside airflow, a model sensitivity test is performed without mountains (NM). A model sensitivity test is also performed to determine the impact of surface friction

for the development of the westerly reversed flow in the lee by removing the mountains and surface friction (NMNF). In addition to land surface heating, the warming on the leeside slopes is a combination of adiabatic warming due to descending airflow in the lee and the latent heat release due to persistent orographic precipitation. A model sensitivity test is also performed by turning off latent heating (NOLH).

Westerly reversed flow is simulated in the wake zone off the Waianae coast in the afternoon hours averaged over the two-month period. Along the windward coast, wind speeds in the control (CTRL) and the NM runs are 5–6 and 6–7 m s^{-1} , respectively. For the No Mountains (NM) run, the wind speeds in the afternoon hours at central Oahu are stronger (4.5–6 m s^{-1} ; Fig. 18b) as

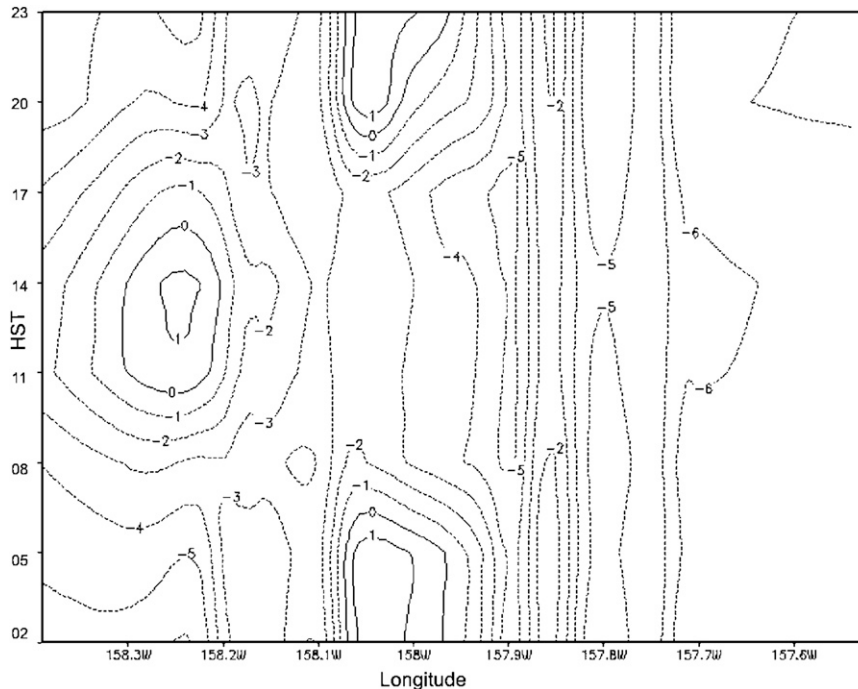


FIG. 16. Mean simulated zonal winds (m s^{-1}) at the surface along 21.45°N throughout the diurnal cycle.

compared with the CTRL run ($3.5\text{--}5 \text{ m s}^{-1}$; Fig. 18a). In the NM case, the afternoon onshore flow and westerly flow offshore still exist. It is apparent that with slower wind speed over land than over the open ocean, due primarily to surface friction, thermally driven westerly flow could still develop along the western leeside coast without orographic effects. Note that westerly flow is not simulated in the wake for the mean flow (Fig. 5).

The surface pressure anomalies from the upstream value at the same height (21.67°N , 157.71°W) at 1400 HST for the CTRL run have slightly positive values on the central and northern windward side and maximum in negative value ($< -0.6 \text{ hPa}$) on the leeside of the Ko'olau Mountains (Fig. 18c). The largest negative anomalies ($< -0.6 \text{ hPa}$) are found over Central Oahu and the foothills of the Waianae Mountains. Relative small negative surface pressure anomalies (-0.2 to -0.4 hPa) were found along the leeside coast as the westerly reversed flow (Fig. 18a) brings in cooler air from the ocean. For the NM run, the negative surface pressure anomalies increase as the air parcels move across the island (Fig. 18d) as a result of land surface heating, with large horizontal gradients where the incoming easterly trades over land converge with the leeside sea breezes inland (Fig. 18b).

For the NMNF run (no mountains and no surface friction), the sea breezes offshore of the western leeside coast are still simulated (Fig. 19a). However, in the

absence of surface friction, winds over central Oahu in the NMNF run are stronger ($> 7.5 \text{ m s}^{-1}$) than the NM run. With stronger incoming winds, the sea breezes in the lee have a smaller north-south extent, and barely move inland over the northwestern coast. The largest negative surface pressure anomalies ($< -0.7 \text{ hPa}$) occur along the western leeside coast (Fig. 19c) before the incoming easterly winds converge with the sea breezes. For the NOLH run, it is striking that the westerly flow fails to develop along the leeside coast (Fig. 19b) in the afternoon hours. The flow decelerates in the leeside wake zone for the NOLH run. The surface pressure anomalies are slightly positive on the central and northern windward coast with a local negative maximum ($< -0.6 \text{ hPa}$) on the leeside slope of the Ko'olau Mountains due to descending airflow in the lee (Fig. 19d). A local negative minimum axis ($> -0.4 \text{ hPa}$) is diagnosed on the windward slopes of the Waianae Mountains, apparently related to cooling as a result of orographic lifting. The negative surface pressure anomalies over central Oahu and the windward slopes of the Waianae Mountains are larger (-0.6 to -0.7 hPa) in the CTRL run (Fig. 18c) as compared with those in the NOLH run (-0.4 to -0.5 hPa ; Fig. 19d). The larger negative surface pressure anomalies over central Oahu and on the windward slopes of the Waianae Mountains in the CTRL run are a result of latent heat release due to the removal of water vapor by

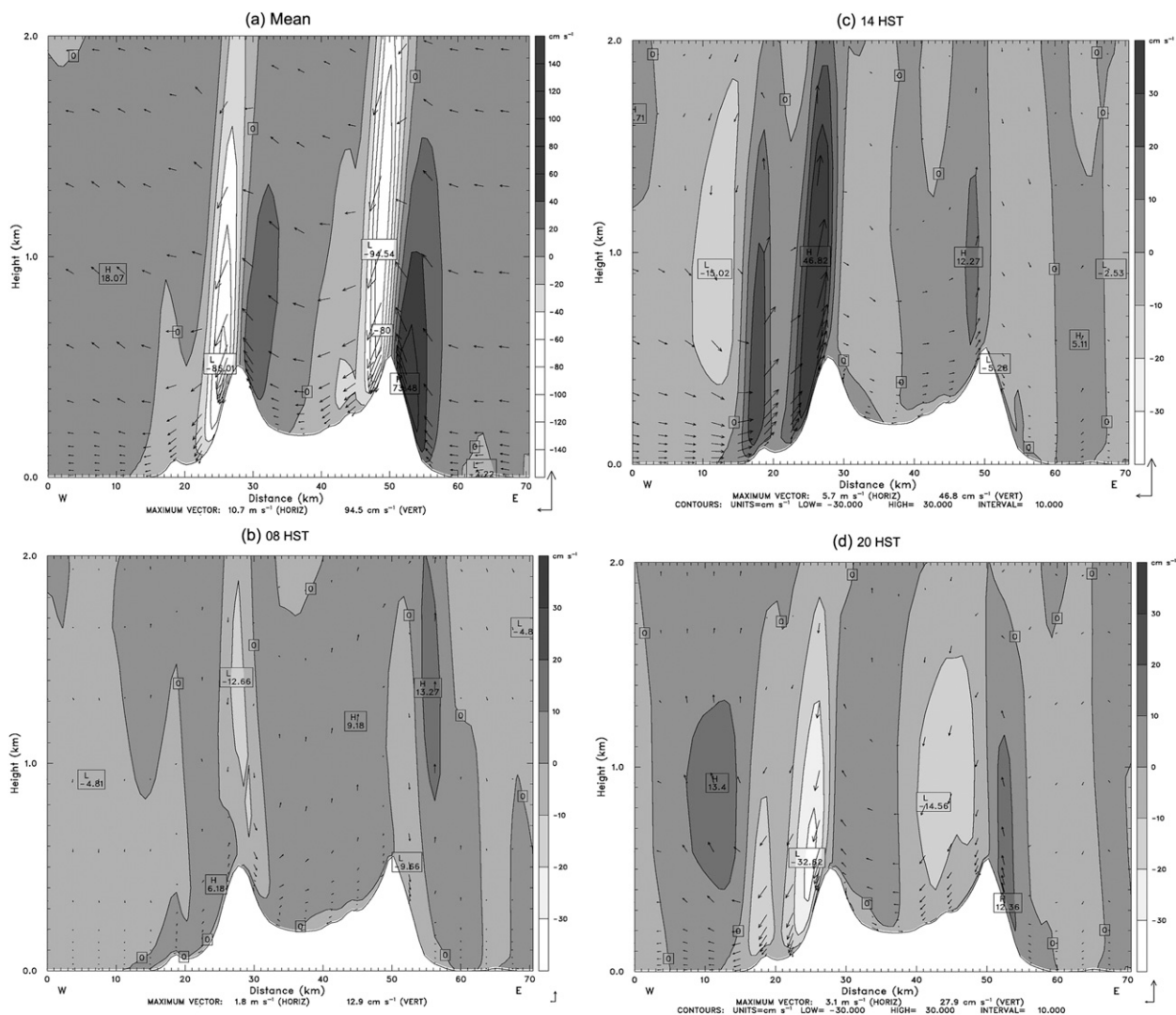


FIG. 17. Vertical cross section of wind vectors ($m s^{-1}$) and vertical velocity (shaded, $cm s^{-1}$) along $21.45^{\circ}N$ for (a) mean state during July–August 2005, and anomalies from the mean at (b) 0800, (c) 1400, and (d) 2000 HST.

persistent orographic lifting by the Ko’olau Mountains as the airflow moves across the island. With the presence of cooling due to orographic lifting on the windward side of the Waianae Mountains, the warming of air parcels moving over the Ko’olau Mountains by latent heating from orographic precipitation has provided the additional warming needed for the development of westerly flow along the leeside coast in the afternoon hours.

The simulated total rainfall accumulation for the CTRL run (Fig. 20a) has a similar spatial distribution as the total rainfall distribution of the two summer months (Fig. 14), with a maximum over the Ko’olau Mountains, a secondary maximum along the leeward slope of the Waianae Mountains, and a minimum over central Oahu. There is no rainfall simulated over the island in the NM

case (Fig. 20b). It is apparent that the terrain is a crucial factor for the development of trade wind showers over Oahu.

8. Summary and conclusions

The MM5/LSM is used to simulate airflow and weather over Oahu during July–August 2005 under summer trade wind conditions. Forecasts from GFS, provided by NCEP, were used to initialize the model. With a 1.5-km resolution, the island effects on airflow and weather are simulated reasonably well for the first time. It is shown that despite its relatively small size ($1536 km^2$), there are considerable spatial variations in horizontal distributions of thermodynamic fields over Oahu related to

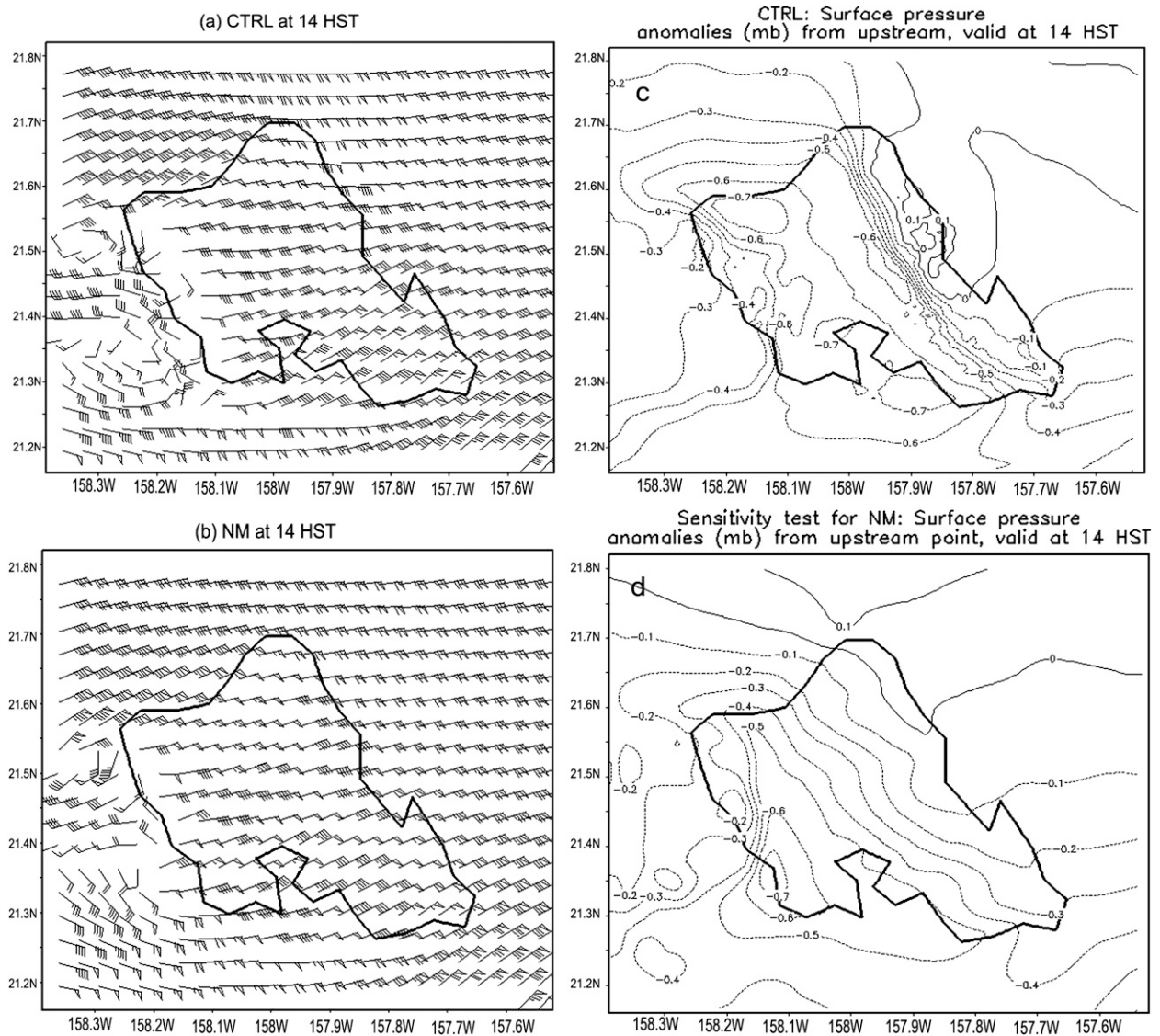


FIG. 18. Simulated wind barbs at 1400 HST 9 Aug 2005 for (a) CTRL and (b) NM. One pennant: 5 m s^{-1} , full barb: 1 m s^{-1} , half barb: 0.5 m s^{-1} , and surface pressure anomalies (hPa) from the upstream value (21.67°N , 157.71°W) at the same height at 1400 HST for (c) CTRL and (d) NM.

terrain, airflow, ground cover, and distributions of cloud and rain. Furthermore, the model results are used to diagnose the physical processes responsible for the observed diurnal variations of rainfall. In addition, model sensitivity tests are performed to diagnose the relative role of thermal forcing versus orographic blocking on the development of the westerly reversed flow in the wake zone off the western leeward coast during the daytime.

Along the windward coast, the temperature and moisture content are comparable to open-ocean values, with relatively small ($\sim 2 \text{ K}$) diurnal variations. The largest diurnal variations in temperature and moisture occur mainly in the lee sides of mountains. During the daytime, there

are large spatial variations in surface temperature anomalies as compared to the upstream values at the same height, with three local maxima ($>6 \text{ K}$): central Oahu, the urban areas of Honolulu along the south shore, and the western central leeward coast. Central Oahu and the south shore are the main urban areas in the lee of the Ko'olau Mountains. The positive temperature anomalies over the ridge tops of the Ko'olau Mountains are smaller ($2\text{--}3 \text{ K}$) than over the Waianae Mountains ($4\text{--}5 \text{ K}$) because of frequent dense orographic clouds and showers, as well as differences in ground cover. The Ko'olau Mountains are covered by tropical forest, whereas the dominant ground covers over the Waianae Mountains are grassland,

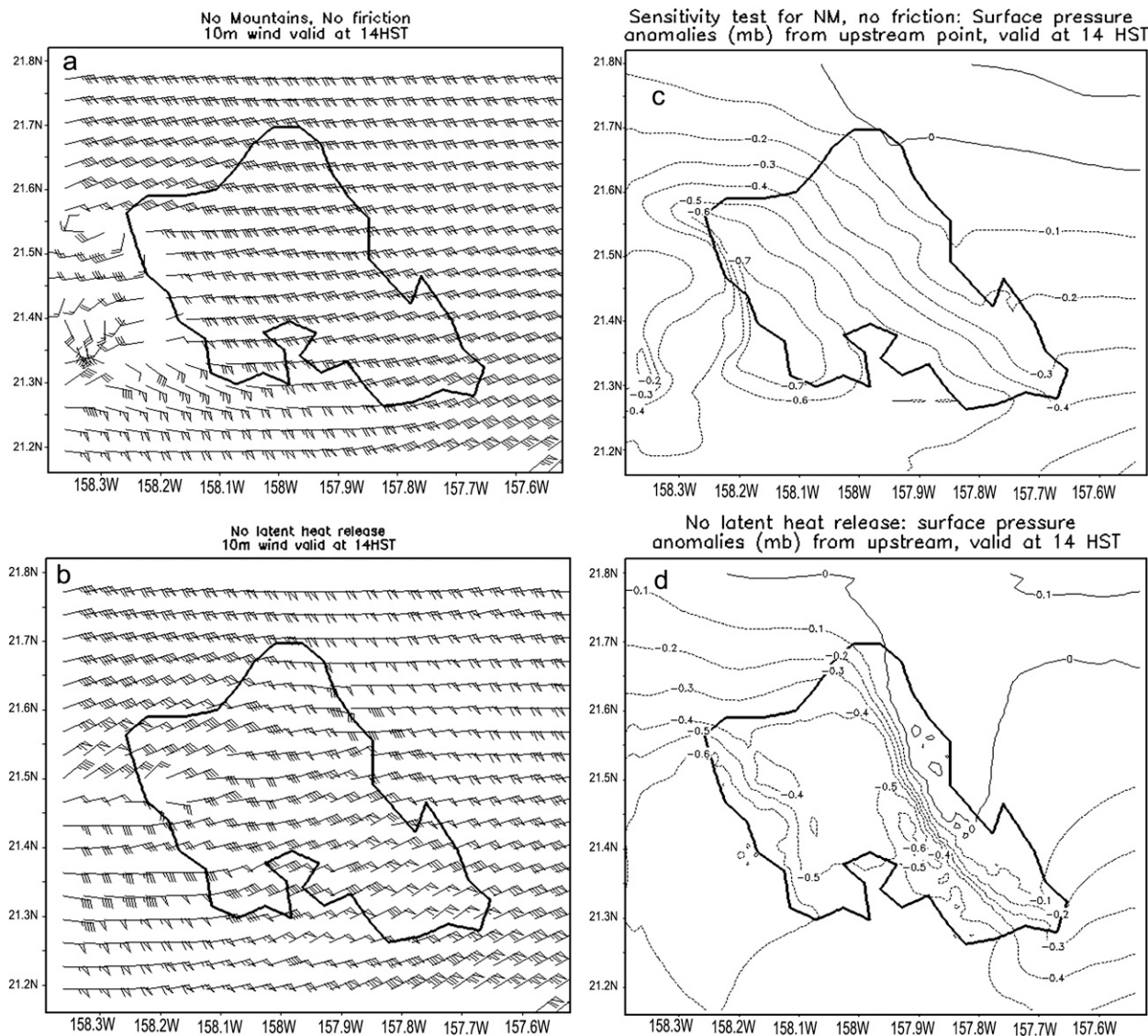


FIG. 19. As in Fig. 18, but for (a) NMNF 10-m wind, (b) NOLH 10-m wind, (c) NMNF surface pressure anomalies (hPa), and (d) NOLH surface pressure anomalies (hPa).

scrubland, and pasture. At night, the largest negative temperature anomalies (< -1.5 K) occur over central Oahu because of weak katabatic flow coming down from the eastern lower slopes of the Waianae Mountains. There is a minimum axis in negative temperature anomalies (> -0.5 K) along the ridge top of the Ko'olau Mountains because of frequent orographic clouds at that location. The smallest negative temperature anomalies occur in the leeside area of the Waianae Mountains and the southeastern leeside areas of the Ko'olau Mountains because of descending airflow in these regions where the terrain is relatively steep with narrow mountain ridges.

During the daytime, a moist axis (> 0.5 g kg⁻¹) is simulated over the Ko'olau Mountains due to orographic

lifting, with relatively dry air downstream. The driest areas (< -1.5 g kg⁻¹) are along the south shore and the central lee side of the Waianae coast as a result of the combined effects of vertical turbulence mixing and descending airflow in the lee. At night, the air is relatively moist with a maximum axis (> 0.5 g kg⁻¹) over the Ko'olau Mountains. The simulated drying along the Waianae leeside coast and south shore at night is less significant (> -0.5 g kg⁻¹) than during the daytime.

Weaker surface winds were simulated over the island interior than over the open. At night, surface winds are weaker than during the day, with katabatic winds over the eastern slopes of the Waianae Mountains and calm winds over central Oahu. Along the windward coast and

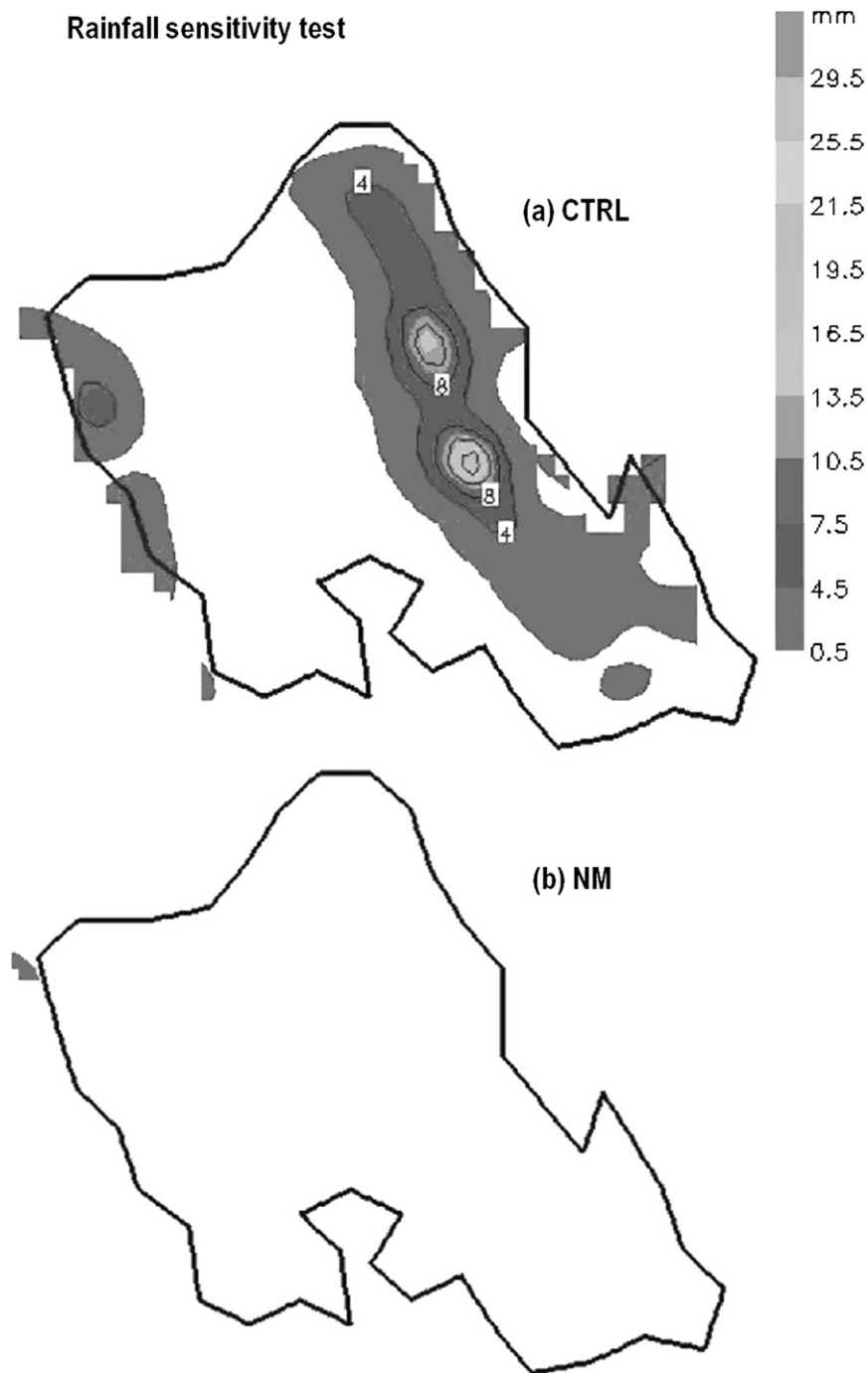


FIG. 20. Total rainfall accumulation (mm) for 9 Aug 2005 for (a) CTRL and (b) NM.

foothills, flow deceleration is most significant in the early morning when the land surface is the coolest. During the day, wind directions are rather uniform over the entire island, with stronger winds than at night due to downward transport of trade wind momentum as a result of vertical mixing. The easterly downslope winds ($>10 \text{ m s}^{-1}$) are

significant above the leeside slopes of both the Ko'olau and the Waianae Mountains at night. The downslope winds in the lee side of the Waianae Mountains are stronger than those above the leeside slope of the Ko'olau Mountains because of higher elevation and steeper leeside slopes. The winds aloft on the leeside slopes of the

Ko'olau Mountains during the day are weaker than at night because of the decrease in stability. Over the lee side of the Waianae Mountains, the downslope winds are replaced by westerly reversed flow in the lowest levels during the day.

Orographic precipitation is frequent over the Ko'olau Mountains and the windward slopes with two simulated diurnal rainfall maxima in agreement with observations. The early morning rainfall maximum is caused by anomalous rising motion on the windward side as a result of significant flow deceleration over the windward coastal regions. This may be enhanced by cloud-top radiative cooling as suggested by previous authors. The early evening rainfall maximum is caused by stronger winds aloft after sunset. The rainfall minimum in the early afternoon is related to relatively weak orographic lifting due to relatively weak winds aloft and a relatively high daytime LFC.

Model sensitivity tests show that in the afternoon, without mountains and surface friction (NMNF case), westerly reversed flow is simulated off the western Waianae leeward coast in the wake zone because of thermal forcing. In the presence of surface friction, but without mountains (NM case), the easterly winds over the island interior are weaker than in the NMNF run ($4.5\text{--}6$ versus $>7.5\text{ m s}^{-1}$), allowing the onshore/westerly reversed flow from the leeward ocean to move onshore and converge with the easterly winds inland. With mountains, but without latent heat release (NOLH case), land surface forcing (daytime heating and surface friction) alone is inadequate for the development of westerly reversed/onshore flow in the wake zone. Cooling due to orographic lifting on the windward side of the Waianae Range is an unfavorable factor for the development of westerly reversed/onshore flow in the wake zone. In summary, the development of daytime westerly onshore/reversed flow in the wake is related to land surface forcing superimposed by latent heat release of orographic precipitation over the Ko'olau Mountains. No rainfall is simulated over Oahu in the NM case, suggesting that persistent orographic lifting is crucial for the development of trade wind showers over Oahu.

Acknowledgments. This work was supported by the USDA Forest Service under Agreement 05-JV-11272165-015. We would like to acknowledge the University of Hawaii/Maui High Performance Computing Center (UH/MHPCC), the Vietnamese Government Project of Training State Officials in Oversea Institutions with the State Budget (Project 322), and the Pacific Disaster Center, Kihei, Hawaii, for funding this research. We would also like to thank Y. Wang, P.-S. Chu, T. Schroeder, and two anonymous reviewers for their comments.

REFERENCES

- Carlis, D. L., Y.-L. Chen, and V. R. Morris, 2010: Numerical simulations of island-scale airflow over Maui and the Maui vortex under summer trade wind conditions. *Mon. Wea. Rev.*, in press.
- Chen, F., and J. Dudhia, 2001: Coupling an advanced land surface-hydrology model with the Penn State-NCAR MM5 modeling system. Part I: Model implementation and sensitivity. *Mon. Wea. Rev.*, **129**, 569–585.
- Chen, Y.-L., and A. J. Nash, 1994: Diurnal variations of surface airflow and rainfall frequencies on the island of Hawaii. *Mon. Wea. Rev.*, **122**, 34–56.
- , and J.-J. Wang, 1994: Diurnal variation of surface thermodynamic fields on the island of Hawaii. *Mon. Wea. Rev.*, **122**, 2125–2138.
- , and J. Feng, 2001: Numerical simulations of airflow and cloud distributions over the windward side of the island of Hawaii. Part I: The effects of trade wind inversion. *Mon. Wea. Rev.*, **129**, 1117–1134.
- Dudhia, J., 1989: Numerical study of convection observed during the Winter Monsoon Experiment using a mesoscale two-dimensional model. *J. Atmos. Sci.*, **46**, 3077–3107.
- , 1993: A nonhydrostatic version of the Penn State-NCAR mesoscale model: Validation tests and simulation of an Atlantic cyclone and cold front. *Mon. Wea. Rev.*, **121**, 1493–1513.
- Epifanio, C. C., and R. Rotunno, 2005: The dynamics of orographic wake formation in flows with upstream blocking. *J. Atmos. Sci.*, **62**, 3127–3150.
- Feng, J., and Y.-L. Chen, 1998: The evolution of katabatic flow on the island of Hawaii during 10 August 1990. *Mon. Wea. Rev.*, **126**, 2185–2199.
- Giambelluca, T. W., M. A. Nullet, and T. A. Schroeder, 1986: *Rainfall Atlas of Hawaii*. Department of Land and Natural Resources Hawaii, Rep. R76, 267 pp.
- Grell, G. A., 1993: Prognostic evaluation of assumptions used by cumulus parameterizations. *Mon. Wea. Rev.*, **121**, 764–787.
- Hartley, T., and Y.-L. Chen, 2010: Characteristics of summer trade wind rainfall over Oahu. *Wea. Forecasting*, in press.
- Hong, S.-Y., and H. L. Pan, 1996: Nonlocal boundary layer vertical diffusion in a medium-range forecast model. *Mon. Wea. Rev.*, **124**, 2322–2339.
- Hsie, E.-Y., R. A. Anthes, and D. Keyser, 1984: Numerical simulation of frontogenesis in a moist atmosphere. *J. Atmos. Sci.*, **41**, 2581–2594.
- Juang, H. H.-M., 2000: The NCEP mesoscale spectral model: A revised version of the nonhydrostatic regional spectral model. *Mon. Wea. Rev.*, **128**, 2329–2362.
- Lavoie, R. L., 1974: A numerical model of trade wind weather on Oahu. *Mon. Wea. Rev.*, **102**, 630–637.
- Leopold, L. B., 1948: Diurnal weather patterns on Oahu and Lanai, Hawaii. *Pac. Sci.*, **2**, 81–95.
- , 1949: The interaction of trade wind and sea breezes, Hawaii. *J. Meteor.*, **6**, 312–320.
- Loveridge, E. H., 1924: Diurnal variations of precipitation at Honolulu, Hawaii. *Mon. Wea. Rev.*, **52**, 584–585.
- Ramage, C. S., and N. E. Oshiro, 1977: Kauai wind power survey—Part I: Mobile sampling program 19, August to September 1977. Department of Meteorology, University of Hawaii Rep. UHMET 77-05, 33 pp.
- Rotunno, R., V. Grubisic, and P. K. Smolarkiewicz, 1999: Vorticity and potential vorticity in mountain wakes. *J. Atmos. Sci.*, **56**, 2796–2810.

- Schär, C., and R. B. Smith, 1993: Shallow-water flow past isolated topography. Part I: Vorticity production and wake formation. *J. Atmos. Sci.*, **50**, 1373–1400.
- , and D. R. Durran, 1997: Vortex formation and vortex shedding in continuously stratified flows past isolated topography. *J. Atmos. Sci.*, **54**, 534–554.
- Schroeder, T. A., 1993: Climate controls. *Prevailing trade winds*, M. Sanderson, Ed., University of Hawaii Press, 12–36.
- , B. Kilonsky, and B. Meisner, 1977: Diurnal variation in rainfall and cloudiness. Water Resources Research Center Tech Rep. 112, 67 pp.
- Smolarkiewicz, P. K., and R. Rotunno, 1989: Low Froude number flow past three-dimensional obstacles. Part I: Baroclinically generated lee vortices. *J. Atmos. Sci.*, **46**, 1154–1164.
- , R. M. Rasmussen, and T. L. Clark, 1988: On the dynamics of Hawaiian cloud bands: Island forcing. *J. Atmos. Sci.*, **45**, 1872–1905.
- Wang, J.-J., H.-M. H. Juang, K. Kodama, S. Businger, Y.-L. Chen, and J. Partain, 1998: Application of the NCEP Regional Spectral Model to improve mesoscale weather forecasts in Hawaii. *Wea. Forecasting*, **13**, 560–575.
- Woodcock, A. H., 1975: Anomalous orographic rains of Hawaii. *Mon. Wea. Rev.*, **103**, 334–343.
- Yang, Y., and Y.-L. Chen, 2008: Effects of terrain heights and sizes on island-scale circulations and rainfall for the Island of Hawaii during HaRP. *Mon. Wea. Rev.*, **136**, 120–146.
- , —, and F. M. Fujioka, 2005: Numerical simulations of the island-induced circulations for the island of Hawaii during HaRP. *Mon. Wea. Rev.*, **133**, 3693–3713.
- Zhang, Y., Y.-L. Chen, S.-Y. Hong, H.-M. H. Juang, and K. Kodama, 2005a: Validation of the coupled NCEP mesoscale spectral model and an advanced land surface model over the Hawaiian Islands. Part I: Summer trade wind conditions and a heavy rainfall event. *Wea. Forecasting*, **20**, 847–872.
- , —, and K. Kodama, 2005b: Validation of the coupled NCEP mesoscale spectral model and an advanced land surface model over the Hawaiian Islands. Part II: A high wind event. *Wea. Forecasting*, **20**, 873–895.

Copyright of Monthly Weather Review is the property of American Meteorological Society and its content may not be copied or emailed to multiple sites or posted to a listserv without the copyright holder's express written permission. However, users may print, download, or email articles for individual use.